A Numerical Study of Mixed CO2-Water Co-Injection into Low Enthalpy Geothermal Systems

David Bennich

Abstract

A Numerical Analysis on the Effects of Using CO$_2$ as a Driving Fluid for a Geothermal Plant
David Bennich

To limit the effect of global warming society needs clean energy sources and to reduce emissions of greenhouse gases into the atmosphere. By combining carbon capture and storage technologies together with geothermal power production it is possible to gain fossil free energy while potentially storing CO$_2$ at the same time. Furthermore, it would be possible to reduce the emissions from geothermal sites with high greenhouse gas content in the groundwater by recirculating the retrieved fluid. Many uncertainties remain however about this type of adaptation.

To study this, this master thesis investigated how a geothermal system would be effected by comparing a water injection with 10 % CO$_2$ to a pure water injection. A 2D model over a 1000 m times 1000 m horizontal fracture zone with two boreholes spaced 500 m apart and a injection rate of 1 kg/s was simulated using the iTOUGH2 software with the ECO2N module, designed for numerical simulations regarding geohydrological systems.

In addition to comparing the two injection scenarios stated above, the effects of changing the injection rate, CO$_2$ concentration in the injection fluid, permeability and surrounding pressure as well as introducing salinity and having an initial CO$_2$ saturated liquid phase were investigated as well.

It was concluded that using CO$_2$ in the injection fluid does allow for a large greenhouse gas sequestration while slightly increasing the heat production, but the system experienced a significant pressure increase while doing so. It was suggested that further investigations regarding adjustments of injection rate and concentration of CO$_2$ was to be performed to find an optimal injection strategy, and to study the impact of different salinity concentrations in both the fracture zone and the injection fluid.

Key words: reinjection, two-phase flow, geothermal energy, CO$_2$ sequestration, iTOUGH2, ECO2N.

Department of Earth Sciences, Air, Water and Landscape Science, Uppsala University. Villavägen 16, SE 752-36 UPPSALA.

Referat

En Numerisk Analys av Effekterna av att Använda CO$_2$ som Drivande Fluid i ett Geotermiskt Kraftverk
David Bennich

För att begränsa konsekvenserna av den globala uppvärmningen behöver dagens samhällen tillgång på fossilfri energi och reducera utsläppen av växthusgaser. Genom att kombinera koldioxidlagringsteknik och geotermisk elproduktion är det möjligt att få utsläppsfri energi samtidigt som det lagras CO$_2$. Vidare finns möjligheten att återcirkulera den upphämtade vätskan för geotermiska kraftverk i områden med högt växthusgasinnehåll i grundvattnet, för att på så vis minska utsläppen från dessa kraftverk. Emellertid så återstår det många osäkerheter kring den här typen av implementation.

För att undersöka detta har ett geotermiskt system studerats hur det skulle påverkas av att använda en vatteninjektion med 10 % CO$_2$ i jämförelse mot rent vatten. En 2D modell över en 1000 m x 1000 m horisontell sprickzon med två borrhål 500 m ifrån varandra och en injektionshastighet på 1 kg/s simulerades med modulen ECO2N till mjukvaran iTOUGH2, en mjukvara som är speciellt designat för att numeriskt simulera geohydrologiska system.

Förutom att jämföra de två injektionsscenariorna ovan så undersöktes även hur skillnader i injektionshastigheten, injektionskoncentrationen av CO$_2$, permeabiliteten och sprickzonens tryck samt införandet av salinitet och en initialt CO$_2$ mättad vätskefas påverkade resultatet.

Slutsatsen blev att genom att använda CO$_2$ i injektionsflödet så möjliggörs en stor lagring av CO$_2$ samtidigt som värmeproduktionen ökar något, men med en stor tryckökning i sprickzonen som följd. Det rekommenderades att göra flera undersökningar på justeringar av injektionshastigheten och CO$_2$ koncentrationen för att hitta en optimal injektionsstrategi, samt att studera hur olika salthalter i både sprickzonen och i injektionsfluiden skulle påverka resultatet.

Nyckelord: återinjektion, tvåfasflöde, geotermisk energi, koldioxidlagring, iTOUGH2, ECO2N.

Populärvetenskalig sammanfattning

Förenta nationernas klimatpanel har satt som mål att den globala uppvärmningen bör hållas under +1.5°C i medeltemperatur. Överskrids denna temperaturökning kommer extrema väderfenomen, torka och kraftig nederbörd att bli allt vanligare med hot mot vattentillgångar, matproduktion och andra mänskliga och naturliga system.

För att motverka den globala uppvärmningen behövs bland annat fossilfria energikällor och även att minska den mängd av växthusgaser som redan finns i atmosfären. Ett sätt att göra detta på är att kombinera geotermisk elproduktion med koldioxidlagringstekniker.

Geotermisk elproduktion använder den värme som finns djupt nere i marken. Genom att injektera vatten i en sprickzon, låta vattnet absorbera den värme som finns och sedan pumpa upp vattnet igen så kan det uppvärmda vattnet förångas och driva en turbin för elproduktion eller användas för varmvatten-produktion. Sådana här anläggningar producerar CO_2, men genom att återinjektera växthusgasen kan geotermiska kraftverk minska sin klimatpåverkan och potentiellt även lagra CO_2 från andra källor.

Frågorna som undersöktes i detta examensarbete är: Hur skulle sprickzonen reagera om 10 % CO_2 började användas i injektionsflödet jämfört med rent vatten? Hur skulle värmeproduktion påverkas, och hur mycket CO_2 skulle potentiellt kunna lagras med en sådan här tillämpning?

För att undersöka detta har processerna i berggrund simulerats med iTOUGH2, en mjukvara som är designad för att hantera geohydrologiska system. Studien genomfördes genom att bygga en 2D modell över en horisontell sprickzon nere i marken. En injektionspunkt och en produktionspunkt placerade 500 m ifrån varandra, och 50 år av verksamhet med 1 kg/s injektions- och produktionsflöde simulerades.

Värmeproduktion ökade när CO_2 användes i injektionsflödet, och många kiloton av växthusgasen fanns i systemet i slutet av simuleringen. Däremot så observerades det stora tryckökningar i sprickzonen, vilket kan leda till skador i berggrunden. För att bedöma hur mycket tryckökning ett system kan hantera innan detta sker kan modellering och experiment genomföras, men detta ligger utanför ramarna för detta examensarbete.

Enklare justeringar injektionshastigheten och CO_2 koncentrationen visade på möjligheten att minska tryckökningen i sprickzonen, och möjligheten finns att hitta en optimal injektionsstrategi för att maximera CO_2 lagring och värmeproduktion med en acceptabel tryckökning.

Vidare så ökade trycket i systemet dramatiskt när 3 % salthalt introducerades vilket troligen beror saltutfällningar som blockerar porer. För att bättre representera verkliga system bör fler simuleringar göras där salthalt varieras i både sprickzonen men även i injektionsflödet då det är ovanligt att injektera med rent vatten.

Slutsatsen drogs att det finns möjlighet att få ren elproduktion med geotermisk kraftproduktion genom att återinjektera den CO_2 som finns i vattnet som pumpats upp från produktionsborrhålet, samt att det finns lagringspotential av växthusgas från externa källor. Särskild uppmärksamhet bör ges till den tryckökning som kommer att ske, genom att analysera att den inte överskrider berggrundens bärkapacitet.

Preface

This master thesis was done in collaboration with the Department of Earth Sciences, Air, Water and Landscape Science at Uppsala University. The thesis corresponds to 30 credits and is the final task of the Master's Programme in Environmental and Water Engineering. The supervisor was Post-Doctoral Farzad Basirat, the supervisor was Professor Auli Niemi and the examiner was Associate Senior Lecturer Alexandru Tatomir, all employed at the Department of Earth Sciences.

I would like to thank Professor Auli Niemi for giving me this assignment and for aiding me as my subject reader. Much appreciation to Linus Wrang for helping with Latex and a huge thank you to Ramin Moghadasi and Farzad Basirat for your guidance in general and assistance with the iTOUGH2 in particular.

Contents

1 Introduction

In IPCC's report from 2018 (IPCC 2018), the need to limit global warming to 1.5°C was heavily emphasized. The current warming has already been observed to increase heavy precipitation, droughts and extreme weather phenomena in different regions, which are damaging to both natural and human systems and a threat the global infrastructure for water and food production among other systems. To successfully limit global warming and its impact the need for transformative system change integrated with sustainable development was deemed essential, and carbon capture and storage (CCS) was recognized as one of the necessary techniques to reach the emission reduction needed.

One promising combination is to use CCS in combination with geothermal power production, by using CO_2 in the injection fluid of a geothermal power plant. This would allow for a clean energy source while simultaneously sequestrating CO_2 underground, providing an answer to society's need to reduce emissions while providing sustainable energy (Brown 2000). Furthermore, it would allow geothermal power plants with high contents of greenhouse gas in the groundwater to diminish their emission rates to the atmosphere by recirculating the extracted fluid (Saldaña et al. 2016).

This report examines the reinjection of CO_2 into a deep geothermal plant, by comparing a pure water and a 10 % CO_2 injection in a two borehole system in a horizontal fracture zone. The questions explored are as follow:

- What happens when CO_2 is injected compared to a pure water injection? How is the heat production, temperature at production point and pressure at injection and production point affected?

- How much CO_2 can potentially be stored?

- How does changing the injection rate, injection concentration, permeability and surrounding pressure influence the results? How does introducing salinity and having an initial CO_2 saturated liquid phase effect the outcome?

2 Background

2.1 Geothermal systems

Geothermal power plants draw their energy from the heat of the Earth. This energy comes from the decay of radioactive isotopes, frictional forces from gravity interactions between the Earth and celestial bodies as well as the crystallization of molten rock (Cresser et al. 2013). The heat energy is most readily available at geologically active zones such as in Iceland and California, while it may require deep boreholes in other parts of the world with a temperature gradient of around 30°C/km (Jelley 2017). In Sweden this temperature gradient ranges from 15°C/km in the northern part of the country to 30°C/km in the south (Erlström et al. 2016).

Since the heat mostly steams from decay of isotopes or the heat from Earths origin, geothermal power is technically not a renewable source (Cresser et al. 2013). Since however the Earth's core is cooling at a very slow rate it is still a viable energy source, as long as the extraction does not overextend the replenishing rate (Cresser et al. 2013).

A geothermal reservoir then is defined as as part of the Earth crust where by using steam, hot water or a mixture of both the reservoirs internal energy can be recovered. There are different types of these reservoirs, each requiring a different conceptual model to study (Toth and Bobok 2017). Water is injected into the reservoir at a high pressure and hot steam is extracted which is used to drive a turbine for power production or used in heat transfer to produce hot water for commercial use (Jelley 2017).

There are three methods used in geothermal power plants: dry steam, flash steam and binary cycle power. Dry steam uses the steam from the reservoir directly to drive the turbine, while flash steam converts hot, high pressure water to steam and usually uses the condensed water as a reinjection fluid. Binary cycle power uses heat transfer between the geothermal fluid to another working fluid (giving it two circular systems, hence the name), which in turn is used for driving the turbine (Administration 2018). Dry and flash steam will emit noncondensable gases (NCG) and produce waste brine while in use, while binary cycle power using its two separate circulations avoids this issue (Cresser et al. 2013).

2.2   Environmental impact of geothermal power production

Greenhouse gases (GHG) are naturally present in geothermal reservoirs and will be emitted during production in dry and flash steam plants. In 2001 the global average of emissions during production was estimated to 122 gCO_2/kWh, with values down to 34 g/kWh in Iceland and up to 1300 g/kWh in southwest Turkey (Fridriksson et al. 2016).

The gases emitted most commonly contains CO_2 and H_2S, and methane, hydrogen, SO_2 and ammonia can also be found and usually in low concentrations (DiPippo 2016). The waste brine can contain high concentrations of calcium, magnesium, chloride and sulphate as well as toxic metals such as cadmium or lead, and must either be treated before release or reinjected (Cresser et al. 2013).

While it is unclear how the emissions will change over the lifespan of a geothermal plan it generally declines with GHG free fluid injection. Furthermore GHG will continuously and naturally emit from geothermal reservoirs by diffusing through soil and steam vents, even without drilling or power production (Fridriksson et al. 2016). So while geothermal power production leads to GHG emissions, it is generally smaller compared to fossil fuel power production and one of the most environmental friendly sources of electricity there is (DiPippo 2016).

2.3   Reinjection of CO_2: Concept and Earlier Modelling

Brown (2000) suggests using supercritical CO_2 to mine heat from a HDR (Hot Dry Rock) reservoir. The report stated that CO_2 in this phase would be nearly as good as water for the heat transfer while simultaneously allowing for a significant sequestering of the greenhouse gas (Brown 2000). In 2014 another report assessed the potential of using CO_2 injection in geothermal reservoirs in China, stating that CO_2 has good mobility and heat capacity while again allowing for trapping of the greenhouse gas (Zhang et al. 2014).

In an conference paper from 2011, geothermal power is referred to as an renewable energy source with zero-emission potential, with current binary cycle plants using total reinjection yielding less than 1 g CO_2/kWh (Goldstein et al. 2011). Furthermore it is stated that geothermal energy is expected to play a key role for mitigating climate changes by displacement of emissions from fossil fuels. The concept of using CO_2 in the injection fluid has therefore already been established since the beginning of the 21st

century as a valid option for geothermal power production while simultaneously reaping the benefits of CO_2 storage.

Work on modelling CO_2 reinjection is already over a decade old. Released in 2006, a study following up Browns report in 2000 of using CO_2 as heat transferring fluid instead of water (Brown 2000) was performed using numerical simulations to explore fluid dynamics and heat transfer issues for a geothermal power plant (Pruess 2006). It was found that CO_2 is superior over water to mine heat from fractured rock, but major uncertainties remained regarding chemical interactions between rock and fluids. The author suggested further investigations on running a EGS with CO_2, stating the concept being "sufficiently attractive".

The oil industry has been using CO_2 injection a long time for enhanced oil and gas recovery. In a study released in 2013 and using the "Tempest" software, a 3D reservoir model were created to study enhanced natural gas recovery combined with CO_2 storage by reinjecting the CO_2 emitted from the production (Khan et al. 2013). It was concluded that using CO_2 injection can increase the gas recovery while simultaneously sequestering large amounts of CO_2.

Moving on to studies regarding using CO_2 for geothermal plants, several of them has looked at the potentiality of using a mixture of water and CO_2 in the reinjection fluid. In order to understand spatial and temporal hydrothermal and chemical effects on targeted geologic media, a model was performed using a flexible approach for solving reactive non-isothermal density-viscosity-dependent flow and reactive transport in low-enthalpy geothermal systems (Nick et al. 2015). If was found that the CO_2 storage in the subsurface might decrease project lifetime due to increased flow rate, but in return enhancing total recovered energy.

Another study a year later wanted to study how to design and operate a reinjection system under various operating conditions. Using the OLGA model a water and NCG reinjection system for high temperature geothermal project was designed, and demonstrated that a single well injection system is a feasible approach with the optimal depth for injection being around 300-500m (Stacey et al. 2016).

To assess the effect of NCG reinjection on energy recovery and permanent trapping of the NCG as well as forecast potential breakthrough, a numerical model of a high temperature reservoir in 3D was set up and studied (Kaya and Zarrouk 2017). While requiring modelling, monitoring and careful well placement in order to avoid premature breakthrough, it was found that reinjecting a mixture of NCG and water can be considered an environmentally friendly disposal method as well as helping with reservoir recharge and improving steam production.

Finally for this study's consideration, two geothermal flash plants with different CO_2 capture techniques were simulated with full reinjection of the geothermal fluid and NCG (Bonalumi et al. 2017). The first plant used the conventional layout of separating and compressing the CO_2 after the condenser, while the other used a new layout which allows separation of CO_2 at higher pressure and thereby reducing the requested power consumption. The conventional plant performed better at high temperature and lower concentrations of CO_2, while the new layout was better for low temperatures and higher gas content.

3 Theory

3.1 Introduction

Geohydrological systems are multicomponent and multiphase structures. To describe and predict the behaviour of such systems, a model over the bedrock, intact and fractured rock zones as well as energy and mass balance equations are needed. In the system studied for this report, the system is limited to a two-phase flow within a homogeneous fractured rock zone. Following in this section, descriptions of two-phase flow, CO_2 solubility and heat transfer as well as the main equations used in the iTOUGH2 software will be discussed.

3.2 Two-phase flow in porous media

A two-phase flow is defined as a flow through a porous media where the two fluids are separated by an interface. The two fluids may flow in different pores or share a pore space, which in the latter during steady flow the fluids might flow in union or one is moving while the other remains stationary. Countercurrent displacement of one fluid by the other is possible, but steady counterflow cannot be realized in a pore system. Furthermore the fluids might both flow continuously, or one might be dispersed in the other as a discontinuous flow (Francis A.L. Dullien 1988).

An important aspect of determining the form of the two phase flow is capillarity. Capillarity is the rise or depression of a liquid in a small passage (Encyclopedia Britannica 2019), and can be described as depending on the contact or wetting angle between the fluids and surface area and the surface tension. This may be described as:

$$P_c = P'' - P' = \left(\frac{2\sigma}{R}\right) cos\,(\theta + \phi) \tag{1}$$

where P$_c$ is the capillary pressure, P' and P" are the hydrostatic pressure of the two fluids, σ is the surface tension, R is the mean pore radius, θ is the contact angle and ϕ is the mean half angle of convergence of the pore walls (Francis A.L. Dullien 1988).

If limited to viscous flow (Reynolds number less than 1) and assuming Newtonian fluids, absence of any physical and chemical change, no slip for gases and isotropic media the Darcy's law may be used to describe a two-phase flow as the following:

$$Q_i = \left(\frac{k_i A}{\mu_i}\right)\left(\frac{\Delta P_i}{L}\right). \tag{2}$$

Q$_i$ is the volumetric flow rate, k$_i$ is the effective permeability, A is the cross-sectional area μ_i is the dynamic viscosity of fluid phase i, ΔP_i the pressure drop and L is the length of the current section. Furthermore, it is customary to introduce relative permeability as

$$k_{ri} = \frac{k_i}{k} \tag{3}$$

where k is the permeability, and to rewrite equation 2 to

$$Q_i = \left(\frac{k_{ri}kA}{\mu_i}\right)\left(\frac{\Delta P_i}{L}\right). \tag{4}$$

Darcy's law may be further generalized by assuming that the equation applies everywhere in the porous media and even in non-steady flow to:

$$\vec{u}_i = -\left(\frac{k_{ri}k}{\mu_i}\right)(\nabla P_i - \varrho_i \vec{g}) \tag{5}$$

where $\vec{u}_i = (\delta Q_i/\delta A)\vec{n}$, $\vec{n}$ is the unit vector for A, $\vec{g}$ is the gravitational vector and ϱ_i is the density of fluid i.

Equation 5 allows the pore system to be divided into small blocks where u_i, P_i, k_{ri} k, ϱ_i and μ_i can be approximated to constant values for each block, while allowing the Darcy's law to remain true on a macroscopic scale for each block. Furthermore gravity is introduced which is standard in hydraulics (Francis A.L. Dullien 1988).

3.3 CO$_2$ solubility in water

Based on a slightly modified version of the correlations developed in Spycher and Pruess (2005), the solubility of CO$_2$ in the aqueous phase is modelled as a function of temperature, pressure and salinity. The CO$_2$ mole fraction x_{CO_2} is described as

$$x_{CO_2} = \frac{\Phi_{CO_2}(1 - y_{H_2O})P_{tot}}{55.508\gamma'_x K^0_{CO_2(g)}}exp\left(-\frac{(P - P^0)\bar{V}_{CO_2}}{RT}\right) \tag{6}$$

where y_{H_2O} is the water mole fraction in the CO$_2$-rich phase and is expressed as:

$$y_{H_2O} = \frac{K^0_{H_2O}a_{H_2O}}{\Phi_{H_2O}P_{tot}}exp\left(\frac{(P - P^0)\bar{V}_{H_2O}}{RT}\right). \tag{7}$$

K^0 is the thermodynamic equilibrium constant at temperature T and reference pressure $P^0 = 1$ bar for each component, P is the pressure, P_{tot} is the total pressure, $\bar{V}$ is the average partial molar volume, Φ is the fugacity coefficient and R is the gas constant. The effect of dissolved salt is expressed through the activity of liquid water a_{H_2O} and the activity coefficient for aqueous CO$_2$ γ'_x (Spycher and Pruess 2005).

3.4 Heat transfer

Heat transfer in a porous media depends on convective and conductive processes. These processes depend on interactions between multi-phase fluids and multi-components as well as changes in phase, internal

energy and enthalpy. The heat convection is contributed by thermal energy which is carried by bulk flow and by dispersive mass fluxes, and the heat conduction is driven by temperature gradients and may follow Fourier's law. The heat transfer may be described as:

$$F^T = \sum_i (h_i \rho_i \nu_i) - \sum_i \sum_k (h_i^k D_i^k \nabla(\rho_i X_i^k)) - (K_T \nabla T) \tag{8}$$

where F^T is the combined heat flux vector, h_i and h_i^k are the specific heat of fluid phase i and component k in fluid i, ρ_i is the density of fluid i, ν_i is the velocity vector of component i, D_i^k is the hydrodynamic dispersion tensor, K_T is the overall thermal conductivity and T is the temperature.

The first two terms describe the heat convection by fluid flow, mass diffusion and dispersion, while the last term concerns the heat conduction. The diffusive fluxes may be neglected in reservoir simulations (Wu 2016).

3.5   iTOUGH2 Simulator and Governing Equations

iTOUGH2 is a numerical simulator based on TOUGH2 and used for parameter estimation, sensitivity analysis and uncertainty propagation analysis (Finsterle 2007). The TOUGH2 framework itself is designed to solve mass and energy balance equations for non-isothermal flow. The software is written in FORTRAN77 and was originally released in 1991. TOUGH2 handles multiphase and multicomponent fluids in a one, two or three dimensional porous and fracture media, and has applications in fields such as geothermal reservoir engineering, waste disposal, saturated and unsaturated hydrology among others (Pruess et al. 2012).

ECO2N is a fluid property module for TOUGH2. Originally designed for studying CO_2 sequestration in saline aquifers, the module includes thermodynamic and thermophysical properties of H_2O - CO_2 - NaCl mixtures and works between the temperature range of $10°C \leq T \leq 110°C$, pressure $P \leq 600$ bar and salinity from zero up to full halite saturation. ECO2N can simulate both isothermal and non-isothermal flow processes and a single or a two-phase flow and allows for phases to disappear or appear throughout the simulation. The fluids are represented as a water-rich liquid phase and a CO_2 rich gas phase, and solid salt might also be present which can precipitate and dissolve. The two chemical processes modelled by ECO2N is the equilibrium phase partitioning of water and CO_2 between the liquid and gas phase, and the precipitation and dissolution of salt (Pruess 2005).

The main mass and balance for an arbitrary flow V_n in TOUGH2 are as follows:

$$\frac{d}{dt} \int_{V_n} M^{(\kappa)} dv = \int_{\Gamma_n} F^{(\kappa)} n d\Gamma + \int_{V_n} q^{(\kappa)} dv \tag{9}$$

where $\kappa=1$ is water, $\kappa=2$ is air and $\kappa=3$ is heat. For $\kappa=1,2$ the mass accumulation terms are:

$$M^{(\kappa)} = \phi \sum_{i=l,g} S_i \rho_i X_i^{(\kappa)} \tag{10}$$

6

where ϕ is porosity, S_i the saturation of phase i, ρ_i the density of phase i and $X_i^{(\kappa)}$ is the mass fraction of component κ in the phase i.

For $\kappa=3$ the heat accumulation is as follow:

$$M^{(3)} = (1-\phi)\rho_R C_R T + \phi \sum_{i=l,g} S_i \rho_i u_i^{(\kappa)} \tag{11}$$

where ρ_R is the rock density, C_R the specific heat, T the temperature and u_i the specific internal energy of phase i.

The mass flux can be described as:

$$F^{(\kappa)} = \sum_{i=l,g} F_i^{(\kappa)} \tag{12}$$

where the flux in each phase is:

$$F_i^{(\kappa)} = -k\frac{k_{ri}}{\mu_i}\rho_i X_i^{(\kappa)}(\nabla P_i - \rho_i g) - \delta_{ig} D_{va}\rho_i \nabla X_i^{(\kappa)} \tag{13}$$

k is the absolute permeability while k_{ri} is the relative permeability of phase i. μ_i is the viscosity of phase i, P is the pressure in phase i and g is the gravitational acceleration. The last term concerns gas flow and D_{va} is the diffusion coefficient for vapor-air mixtures.

The heat flux is described as (assuming no dispersion):

$$F^{(3)} = -K\nabla T + \sum_{i=l,g} \sum_{\kappa=1,2} h_i^{(\kappa)} F_i^{(\kappa)} \tag{14}$$

where K is the heat conductivity of the rock-fluid mixture and $h_i^{(\kappa)}$ is the specific enthalpy of component κ in phase i (Pruess 1987).

4   Method

4.1   Conceptual model

Developed by Bruno Figueiredo, the conceptual model studied was a two wellbore system with an horizontal fracture zone as seen in figure 1a (Figueiredo et al. 2020). An injection and a production point were spaced 500 m apart in a 1000 m x 1000 m fracture zone, surrounded by an 2000 m x 2000 m intact rock zone (figure 1b) and with a thickness of 10 m for the entire model. The rock properties of the intact and fracture zone were selected to represent a geological system at a depth of 7000 m (Figueiredo et al. 2020) and are listed in table 1.

Table 1: *Rock properties*

	Intact rock	Fractured rock
Density	2700 kg/m^3	2700 kg/m^3
Porosity	0.02	0.02
Absolute permeability	10^{-21}	10^{-14}
Heat conductivity (liquid-saturation)	2.9 W/(m °C)	2.9 W/(m °C)
Specific heat	790 J/(kg °C)	790 J/(kg °C)
Pore compressibility	$4.5 \cdot 10^{-10}$	$4.5 \cdot 10^{-10}$

Corey's curves were used for the relative permeability function and can be described as:

$$k_{rl} = \hat{S}^4 \tag{15}$$

and

$$k_{rg} = (1 - \hat{S})^2 (1 - \hat{S}^2) \tag{16}$$

where

$$\hat{S} = (S_l - S_{lr})/(1 - S_{lr} - S_{gr}) \tag{17}$$

and subjected to the restriction:

$$S_{lr} + S_{gr} < 1. \tag{18}$$

Van Genuchten was used for capillary pressure function and is as follow:

$$P_{cap} = -P_0([S^*]^{-1/\lambda} - 1)^{1-\lambda} \tag{19}$$

where

$$S^* = (S_l - S_{lr})/(S_{ls} - S_{lr}) \tag{20}$$

and subjected to the restriction

$$-P_{max} \leq P_{cap} \leq 0. \tag{21}$$

The parameters used for Corey's curves and Van Genuchten are listed in table 2 below (Pruess et al. 2012).

Table 2: *Relative permeability and capillary pressure function parameters*

Corvey's curves		Van Genuchten	
S_{lr}	0.3	λ	0.4
S_{gr}	0.05	S_{lr}	0
		$1/P_0$ (Intact rock)	$1.5 \cdot 10^{-6}$
		$1/P_0$ (Fractured rock)	$2.5 \cdot 10^{-4}$
		P_{max}	$1 \cdot 10^{-4}$
		S_{ls}	1.0
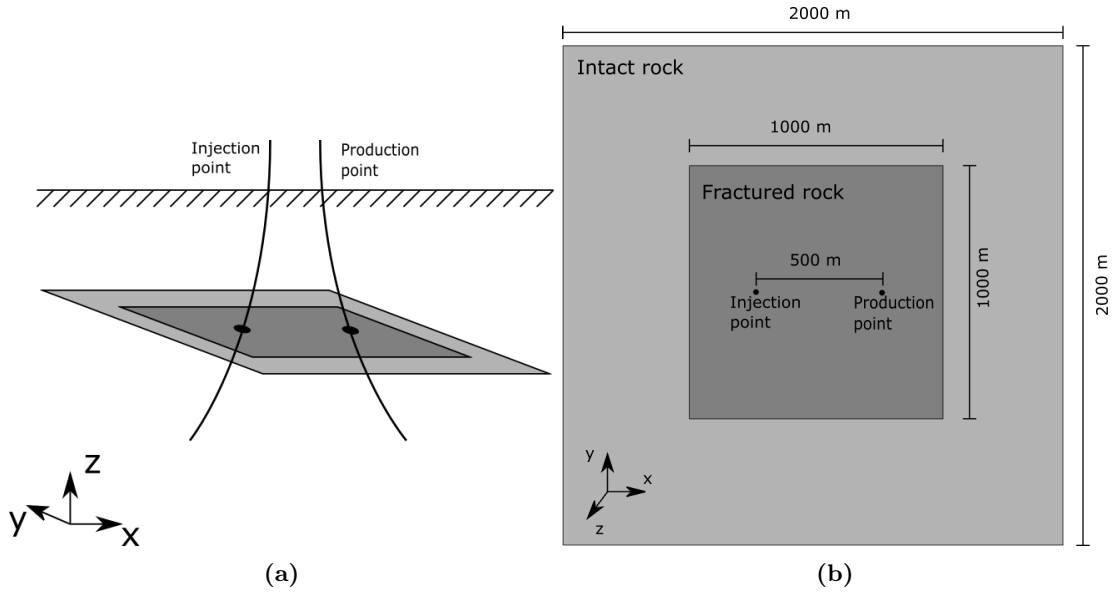
Figure 1: (a) The conceptual model of the wellbore system. The injection borehole is placed close to the production borehole and fluid is injected into a horizontal fracture zone surrounded by intact rock. (b) The horizontal 2D model used for the simulations. One injection and one production point is spaced apart within the dark grey area of fractured rock surrounded by the intact rock in light grey.

A non-flow boundary condition was assumed at the outer boundaries, and the entire model was constructed using 7200 grid elements with the resolution being higher around the wellbore points (see figure 2). The length of the elements at and around the wellbore in x- and y-direction started at 5 m, then increasing to 7.5, 10, 20, 30, 40, 60, 100 and finally to 200 m in size while never extending 20 m between the wellbore points. The thickness was designed using only one grid element of 10 m length, making the model effectively a 2D system.
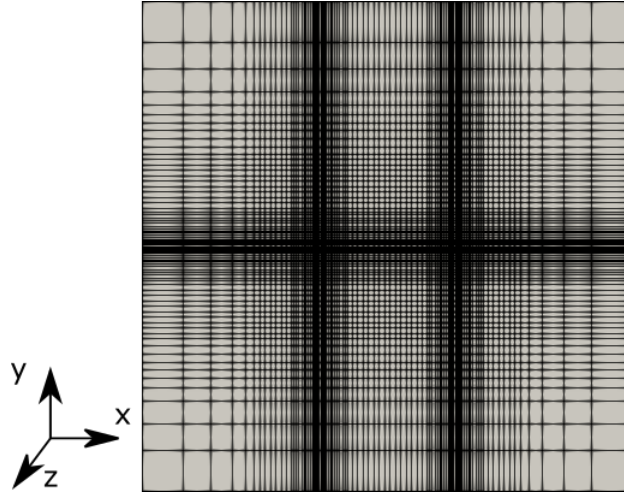
Figure 2: The grid resolution of the model, consisting of 7200 elements. Notice how the resolution is increased around the two wellbore points.

4.2   Simulated cases and analysis

The study consisted of two base case and seven comparative scenarios. The two base case scenarios consisted of one pure water and one 10 % CO_2 injection, both injected at 1 kg/s with a temperature of 80°C in a 300 bar and 100°C environment. For the 10 % CO_2 injection, the model adds 0.1 kg/s of CO_2 and 0.9 kg/s of water at the the injection points and then calculates how much of the CO_2 that dissolves into the water and how much remains as a free gas. Salinity and initial dissolved CO_2 in the fracture zone was set to 0 %, permeability to 10^{-14} m^2 and the simulation ran 50 years to allow for stable conditions to settle. The parameters used are based on Figuereido et al. (2020) and are listed in table 3.

Table 3: *Parameters for the base case scenarios and initial conditions*

Injection rate	1 kg/s
CO_2 injection percentage	10 %
Salinity	0 %
Injection temperature	80°C
Dissolved CO_2	0 %
Permeability	10^{-14} m^2
Pressure	300 bar
Background temperature	100°C
Simulation time	50 years

In the comparative scenarios one parameter at the time was changed as listed in table 3, and simulations were run for both the pure water and the 10 % CO_2 injection. The seven comparative scenarios and what parameter that was modified are listed in table 4.

Table 4: *Parameters for the comparative scenarios*

Injection rate	0.1 and 0.6 kg/s
CO_2 injection percentage	6 %
Salinity	3 %
Injection temperature	60°C
Dissolved CO_2	5.5476 %
Permeability	10^{-12} m^2
Pressure	200 bar

For each scenario the heat production, temperature at production point, pressure at injection and production point and the total mass of CO_2 was plotted over time. For those scenarios whose plots motivated further analyses, contour plots over temperature, pressure and/or CO_2 saturation was added.

5 Results

5.1 Base Case Scenario

Figure 3a and 3b shows the heat production and the temperature at the production point for the base case scenarios. The heat production showed a higher value for the CO_2 injection than the injection with only water, up to about 6 % higher as seen in figure 3a.
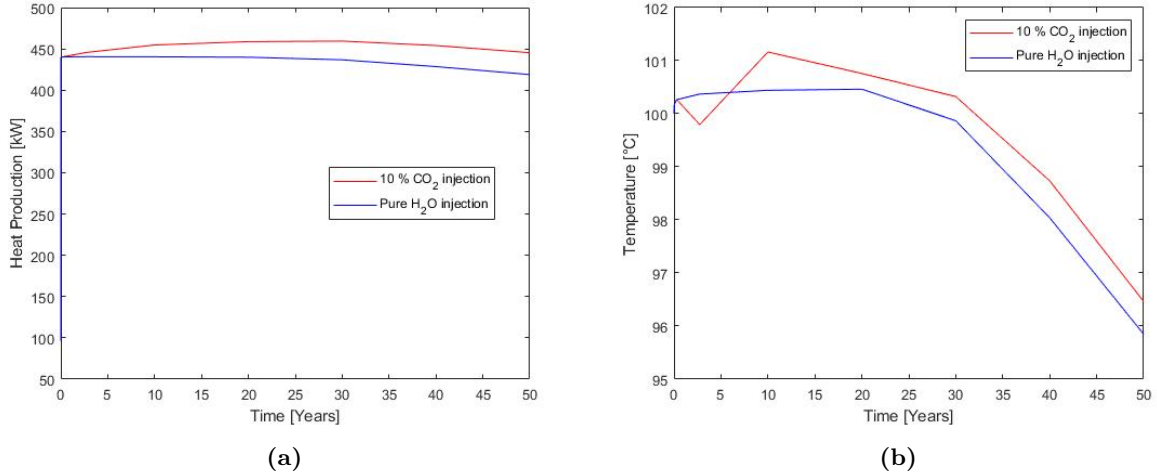
Figure 3: (a) The heat production in kW for the base case scenarios. **(b)** The temperature at the production point for the base case scenarios.

The temperature at the production point (figure 3b) showed an initial oscillating behaviour for the 10 % CO_2 injection base case scenario during the first 10 year of simulation time, to then start declining for the rest of the simulation. The pure water injection exhibits a slow rise for the first 20 years and

then behaves like the CO_2 injection but with a slight negative offset throughout. When looking at the temperature contour plots of the two base cases in figure 7 and 5, it can be seen that the behaviour is overall very similar between them.
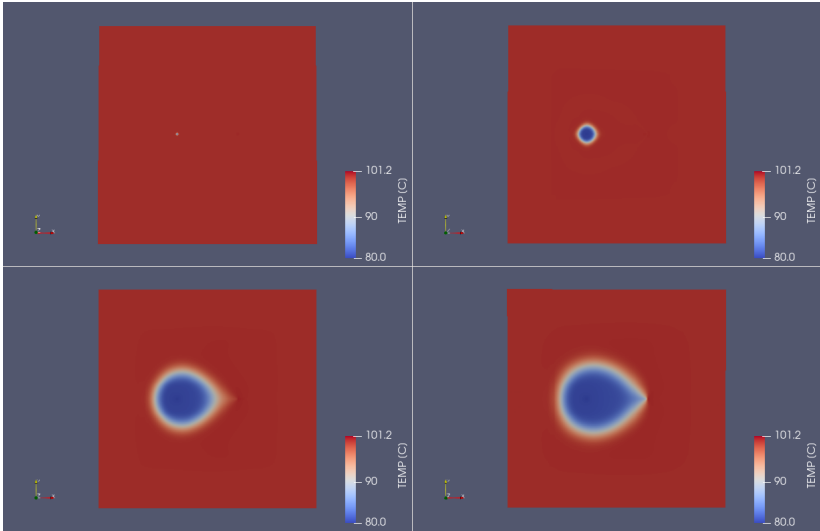
Figure 4: The temperature for the 10% CO_2 base case scenario after 10 days, 1000 days, 30 years and 50 years.

The circular cooling area around the injection points slowly grows for the duration of the simulation with a tail expanding towards the production point as time goes on. The final shape displays the flow path, where the circular expansion at the injection point is drawn towards the production point due to the fluid extraction at that point.
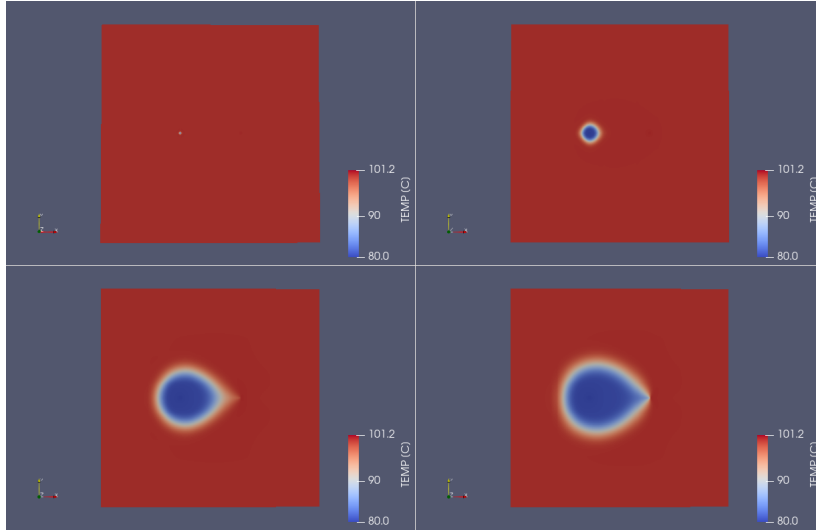
Figure 5: The temperature for the pure water base case scenario after 10 days, 1000 days, 30 years and 50 years.

Figure 6a and 6b shows the pressure at the injection and the production point for the two base case scenarios. The initial jump of pressure in figure 6a and the initial pressure drop in figure 6b are due to numerical considerations.
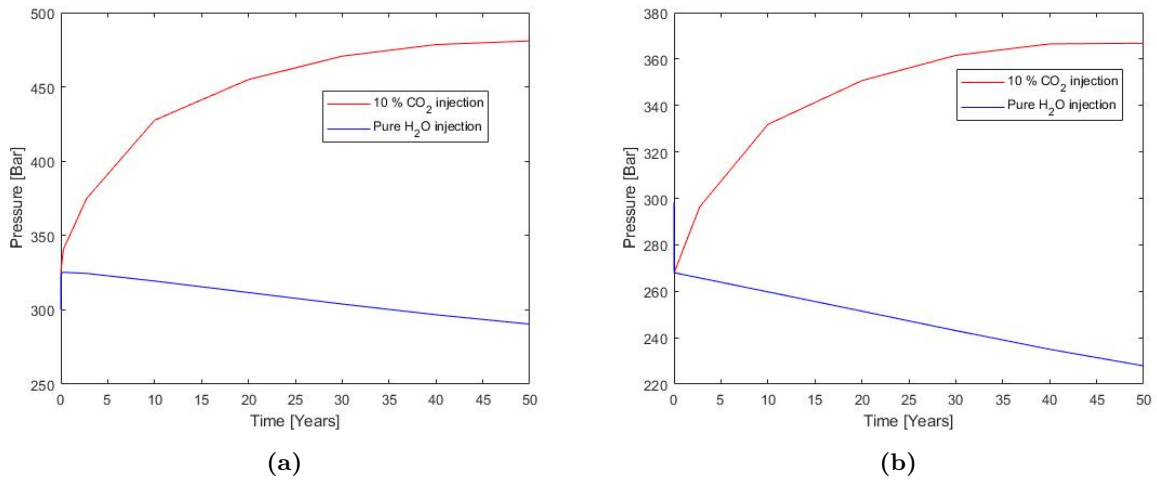
Figure 6: (a) The pressure at the injection point for the base case scenarios. **(b)** The pressure at the production point for the base case scenarios.

The pressure increase throughout the CO_2 injection scenario is due to build-up of free gas and appears to be converging at the simulations end as seen in figure 6a and 6b. This gas build-up and pressure increase is absent for the water injection and instead the pressure linearly decreases. These behaviours for the two base case scenarios are further emphasized in the contour plots in figure 7 and 8.

13
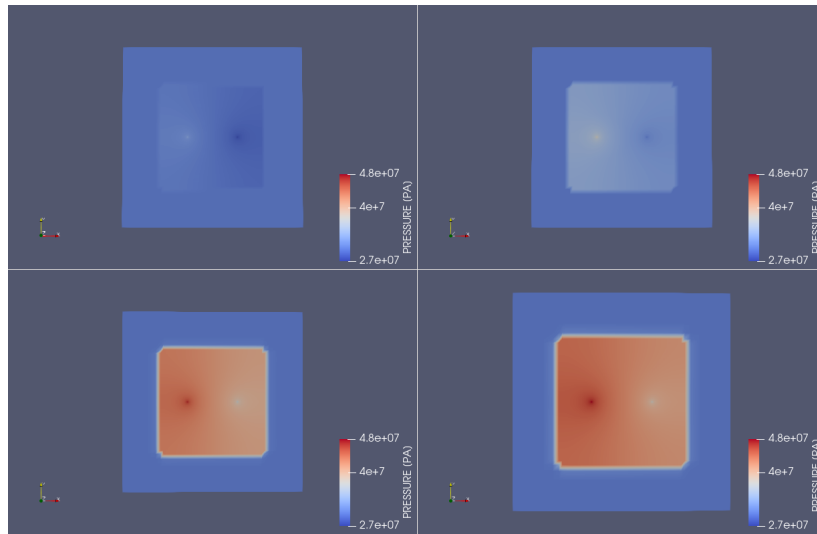
Figure 7: The pressure for the 10% CO_2 injection after 10 days, 1000 days, 30 years and 50 years.

The entire fracture zone for the CO_2 injection shows a pressure increase as seen in figure 7, again because of the build-up of free gas. The pressure increase is the steepest at the injection point and lowest at the production point due the injection and extraction of fluid respectively. For the water injection and with the absence of free gas the fracture zone shows instead an overall decrease in pressure, as seen in figure 8.
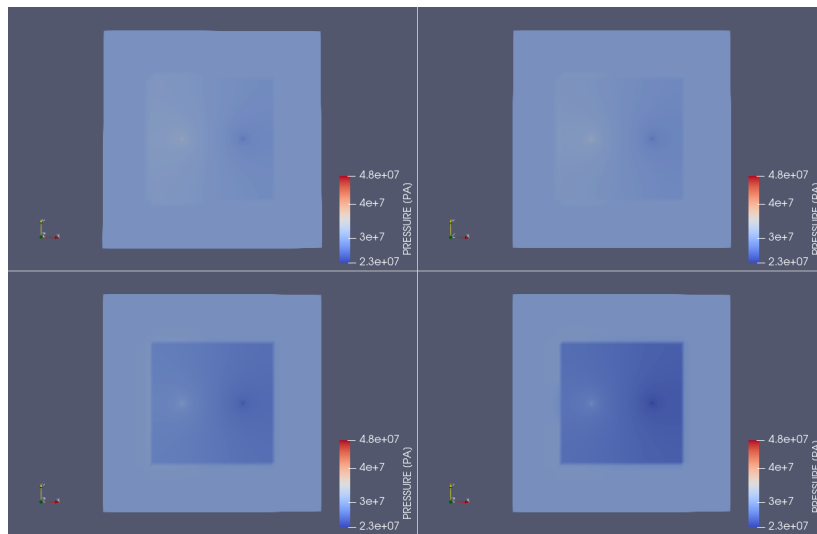
Figure 8: The pressure for the pure water injection after 10 days, 1000 days, 30 years and 50 years.

The gas saturation is seen slowly filling up towards 20 % the entire fracture rock zone, almost covering the zone at the simulation end (figure 9).

14
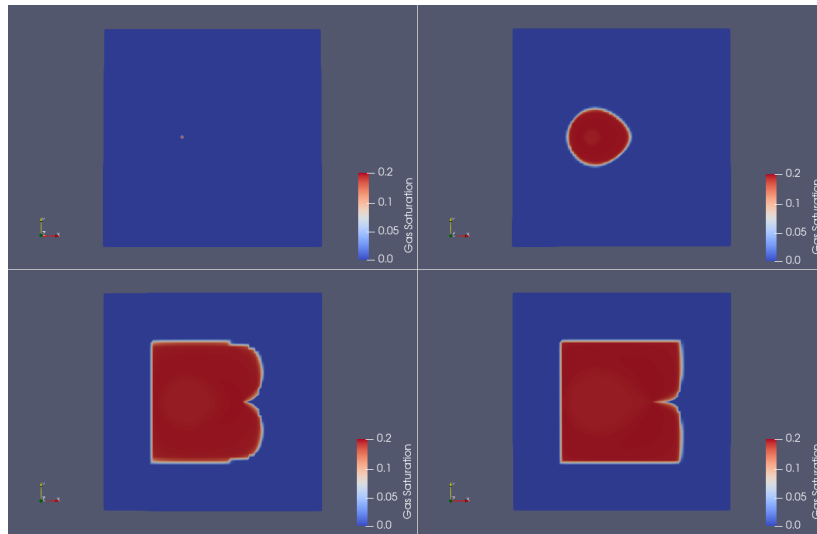
Figure 9: The gas saturation for the 10 % CO_2 injection after 10 days, 1000 days, 30 years and 50 years.

The total mass of CO_2 stored in the system landed at 33.5 kiloton after the 50 year simulation run time (figure 10), and appeared to be close to converging. Furthermore the injected CO_2 is detected at the production point after roughly seven years and nine months of simulation time.
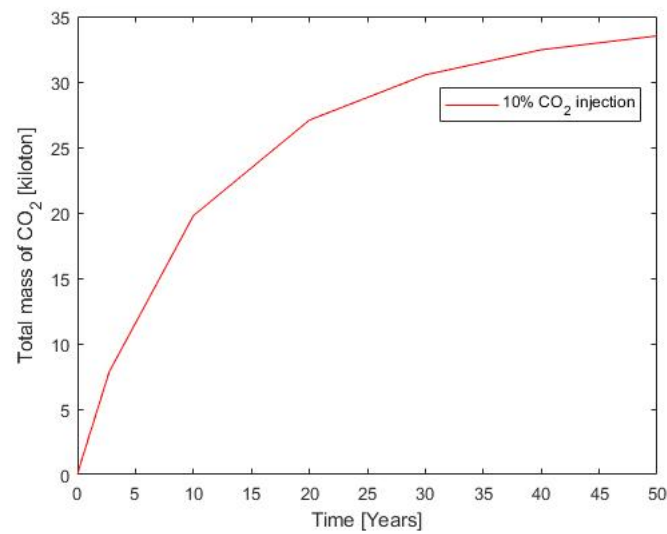
Figure 10: The total mass of CO_2 in the system during the 10 % CO_2 injection base case scenario.

15

5.2 The effect of injection rate

The first comparative scenario studied the effect of lowering the injection rate to first 0.6 and then 0.1 kg/s. The heat production simply increased as the injection rate did (figure 11a), while being indistinguishable for the lowest injection rate between CO_2 and water. The impact of the injection rate is larger than the effect of using 10 % CO_2 compared to pure water, which might be due to the relative large difference between the flow rates when increasing from 0.1 kg/s up to 1.0 kg/s.
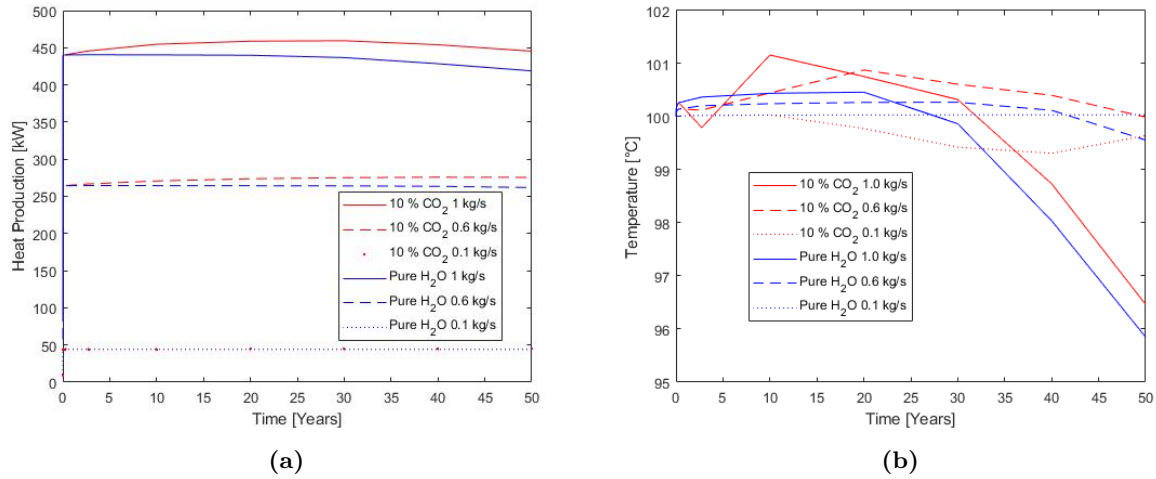
Figure 11: (a) The effect on heat production using 0.1, 0.6 and 1 kg/s injection rate. **(b)** The effect on the temperature at the production point using 0.1, 0.6 and 1 kg/s injection rate.

The temperature at the production point significantly altered its behaviour between the different rates. The water injection rate maintained an initial stable temperature to then decline steeper and earlier during the simulation as the rate increased, and the CO_2 showed oscillating behaviours ranging from an downswing for 0.1 kg/s, upswing for 0.6 kg/s to an complete oscillation for 1 kg/s with a final drop at the simulations end (figure 11b). Looking at the 0.6 kg/s temperature contour plot (figure 12, one sees the behaviour established in figure 4) but to a lesser extent.
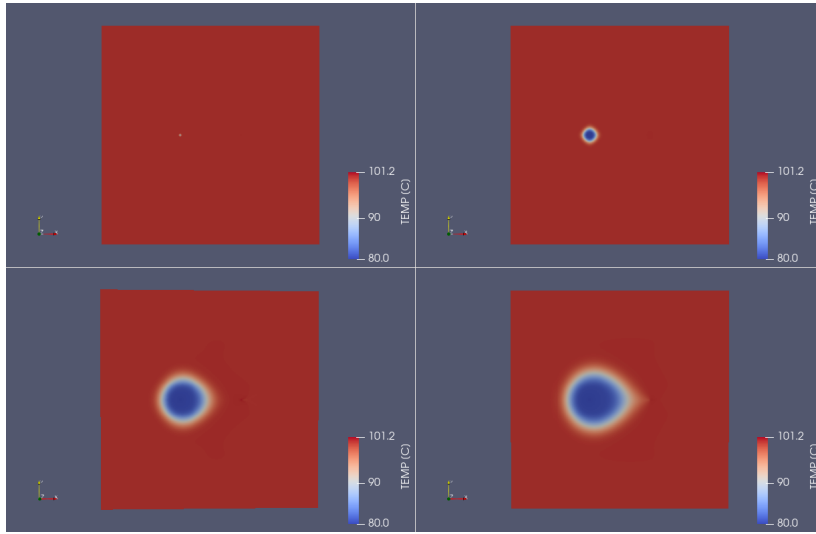
Figure 12: The temperature for the 0.6 kg/s injection rate of 10 % CO_2 after 10 days, 1000 days, 30 years and 50 years.

The pressure was affected differently between the water and CO_2 injection for the different flow rates. The pressure for the 10% CO_2 injection scenarios simple increased as the rate went up due to increasing amounts of free gas in the system. One notable exception was the higher pressure at the production point for the 0.6 kg/s compared to the 1 kg/s rate (13b). The pressure for the water injection scenarios decreased at a faster rate the higher the flow rate, which is likely due to the faster cooling of the system and the reverse thermal expansion that follows.
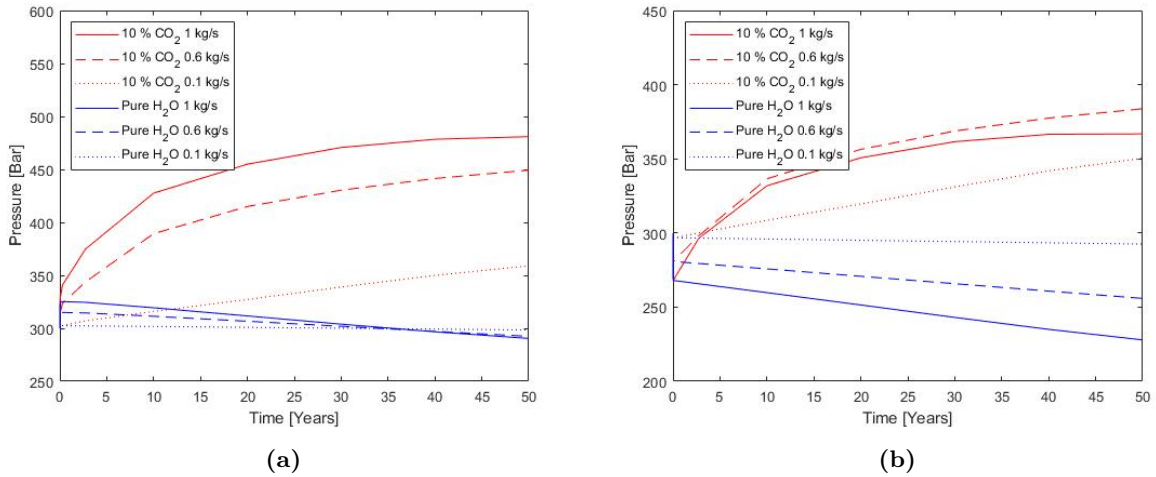
Figure 13: **(a)** The effect on pressure at the injection point using 0.1, 0.6 and 1 kg/s injection rate. **(b)** The effect on pressure at the production point using 0.1, 0.6 and 1 kg/s injection rate.

Similarly to the temperature contour figure, the gas saturation for the 0.6 kg/s injection showed much

17

the same behaviour but to an lesser extent. The fracture zone does not fill out as much at each time print compared to the base case scenario and the overall saturation stays around 15 % (figure 14).
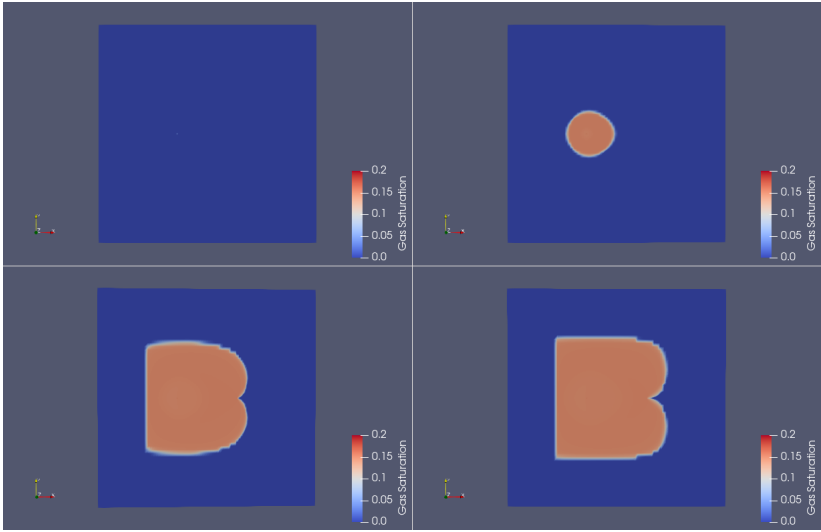
Figure 14: The gas saturation for the 0.6 kg/s injection rate of 10% CO_2 after 10 days, 1000 days, 30 years and 50 years.

The total mass of CO_2 increased as the injection rate went up, but with a declining rate of return as seen in figure 15. This is simply due to more CO_2 being injected into the system the higher the flow rate is chosen.
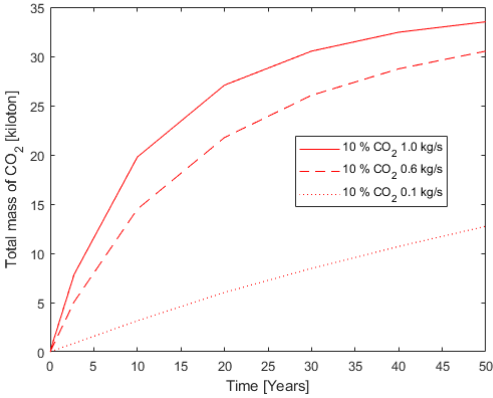
Figure 15: The effect on the total mass of CO_2 stored using 0.1, 0.6 and 1 kg/s injection rate.

18

5.3 The effect of CO$_2$ concentration

The new injection rate simple increased the heat production slightly from the pure water but decreased it slightly from the 10 % CO$_2$, placing the new curve between the two old ones (figure 16a). The temperature curve at the production behaved similar for 6 % as for 10 % CO$_2$, but with slightly lower altitude and delayed peak value (16b).
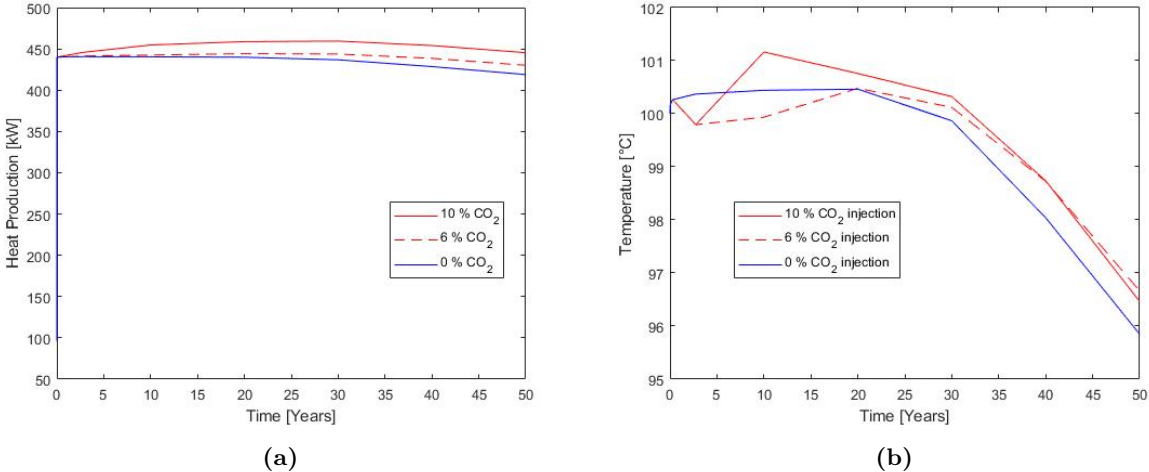
Figure 16: **(a)** The effects on heat production for different CO$_2$ injection concentrations. **(b)** The effects on the temperature at the production point for different CO$_2$ injection concentrations.

The temperature for the entire fracture zone displayed the same behaviour as seen for the 0.6 kg/s injection rate, as the two contour plots are almost indistinguishable (figure 17 below compared to 12 above).
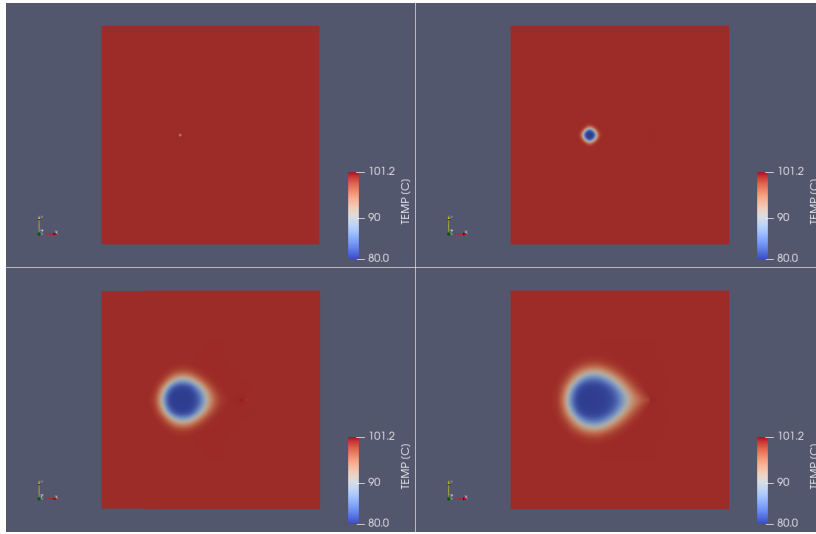
Figure 17: The temperature for the 6 % CO_2 injection after 10 days, 1000 days, 30 years and 50 years.

The pressure curves on the other hand showed no such similarities. The 6 % CO_2 decreased pressure at both borehole points after the initial vertical dislocation, and then slowly increased for the duration of the simulation (figure 18a and 18b).
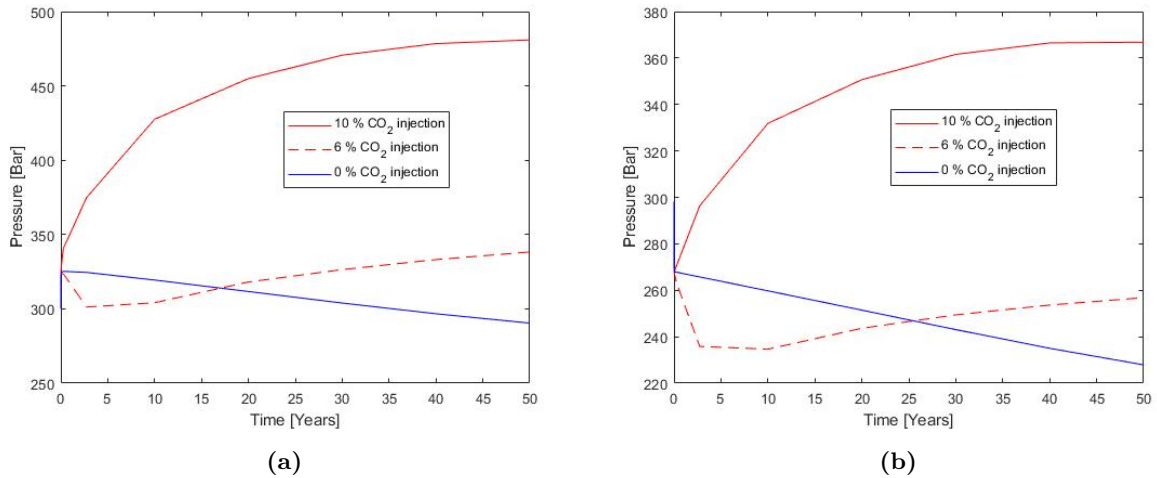
Figure 18: **(a)** The effect of using 6 % CO_2 on the pressure at the injection point. **(b)** The effect of using 6 % CO_2 on the pressure at the production point.

The spread of the gas saturation area between 6 % CO_2 and 0.6 kg/s is almost identical, similarly to that of the temperature contour plots. This time however the gas saturation reaches 20 % as seen in figure 19, which is more aligned to the 10 % CO_2 base case scenario.
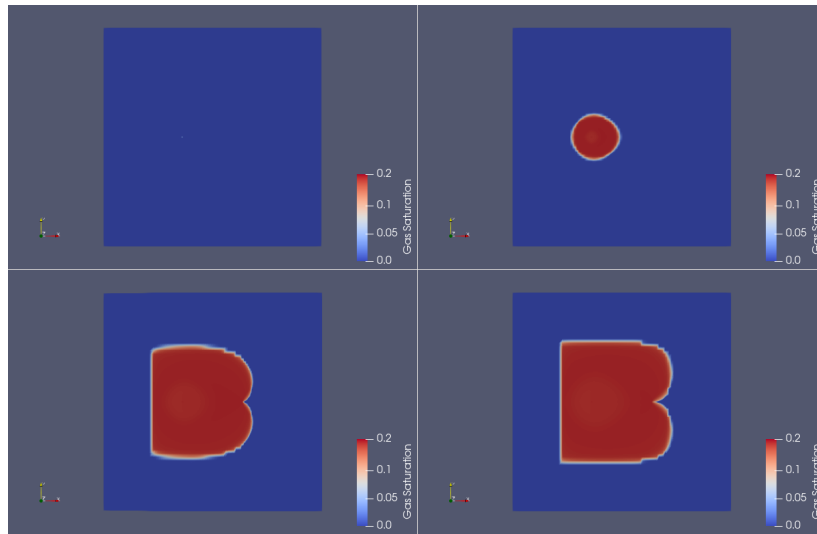
Figure 19: The gas saturation for the 6 % CO_2 injection after 10 days, 1000 days, 30 years and 50 years.

The total CO_2 mass landed on only 53 % compared to the CO_2 base case scenario, despite of having 60 % of the original injection concentration (20).
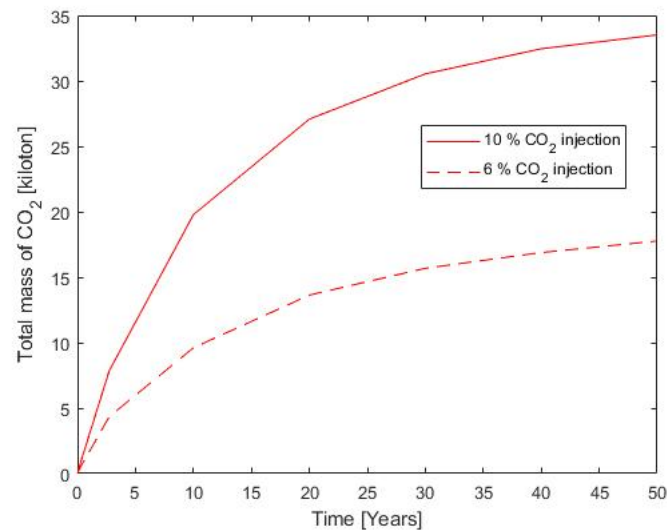
Figure 20: The effect of using 6 % CO_2 on the total amount of CO_2 stored.

5.4 The effect of salinity

Introducing 3 % salinity in the system only slightly increased the heat production (figure 21a) and the temperature at the production point (figure 21b).
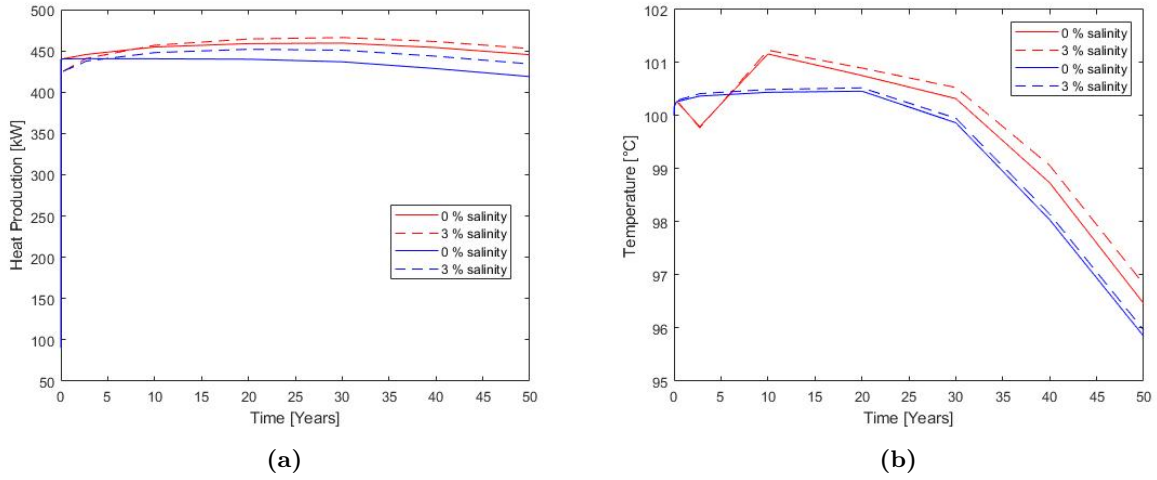
Figure 21: **(a)** The effects of 3 % salinity on heat production for the CO_2 injection in red and pure water in blue. **(b)** The effects of 3 % salinity on the temperature at the production point for the CO_2 injection in red and water in blue.

More dramatically effected was the pressure, skyrocketing for both the water and the 10 % CO_2 injection (figure 22a and 22b).
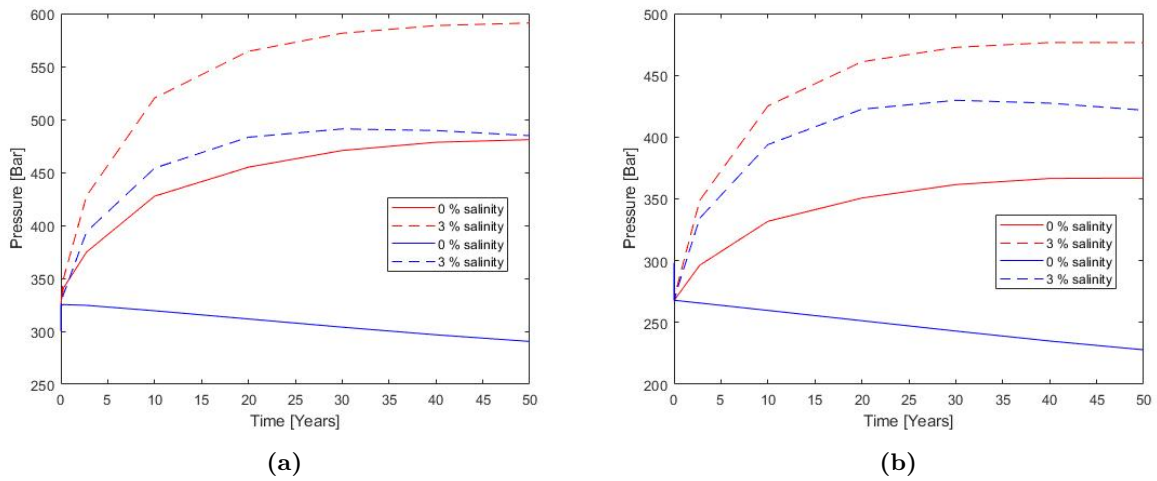
Figure 22: **(a)** The effect of 3 % salinity on the pressure at the injection point with CO_2 injection in red and water in blue. **(b)** The effect of 3 % salinity on the pressure at the production point with CO_2 injection in red and water in blue.

As for the total mass of CO_2 a slight increase was observed (figure 23).
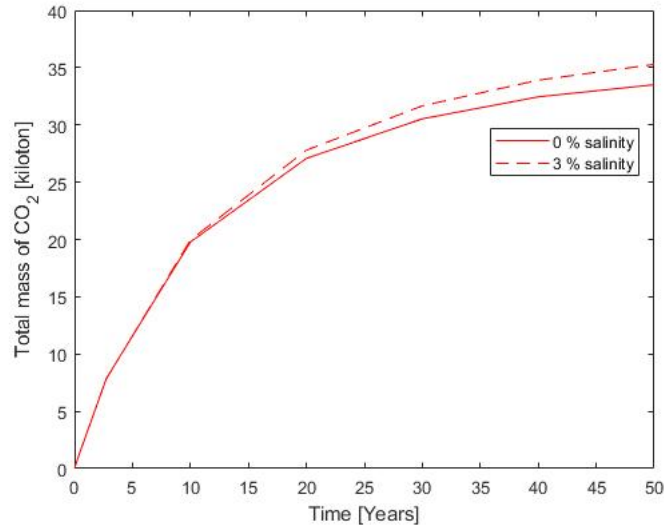
Figure 23: The effect of 3 % salinity on the total amount of CO_2 stored with the CO_2 injection in red.

5.5 The effect of injection temperature

The lowered injection temperature only decreased the heat production slightly (figure 24a) but made clear reduction of the temperature at the production point (figure 24b).

| (a) | (b) |
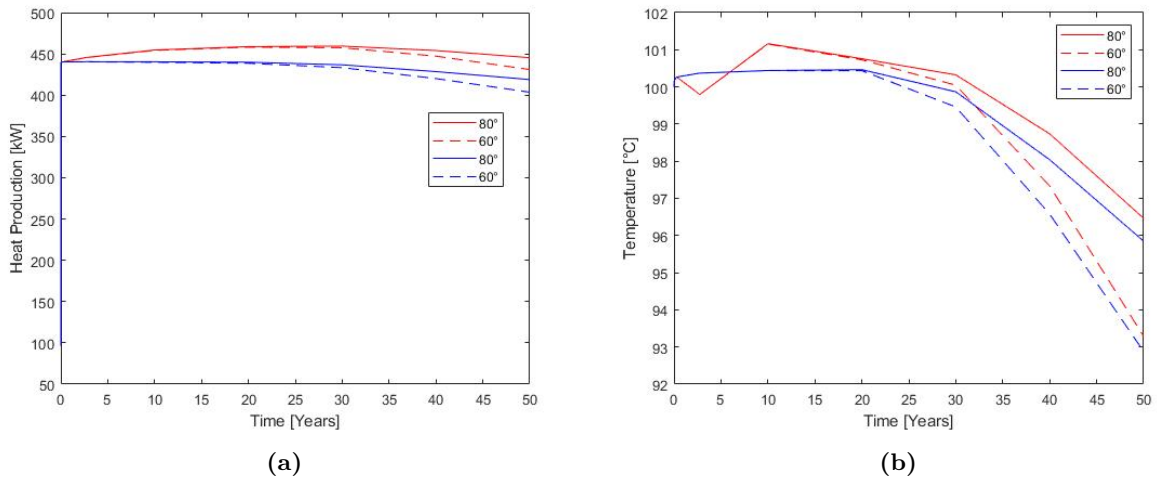
Figure 24: (a) The effect of the 60°C injection temperature on the heat production, with the CO_2 injection in red and water in blue. **(b)** The effect of the 60°C injection temperature on the temperature at the production point, with the CO_2 injection in red and water in blue.

The pressure was more effected for the water than the CO_2 injection, but both showed a moderate

decrease for the lowered injection temperature (figure 25a and 25b). This is likely due to reversed thermal expansion due to the cooling.

(a)

(b)
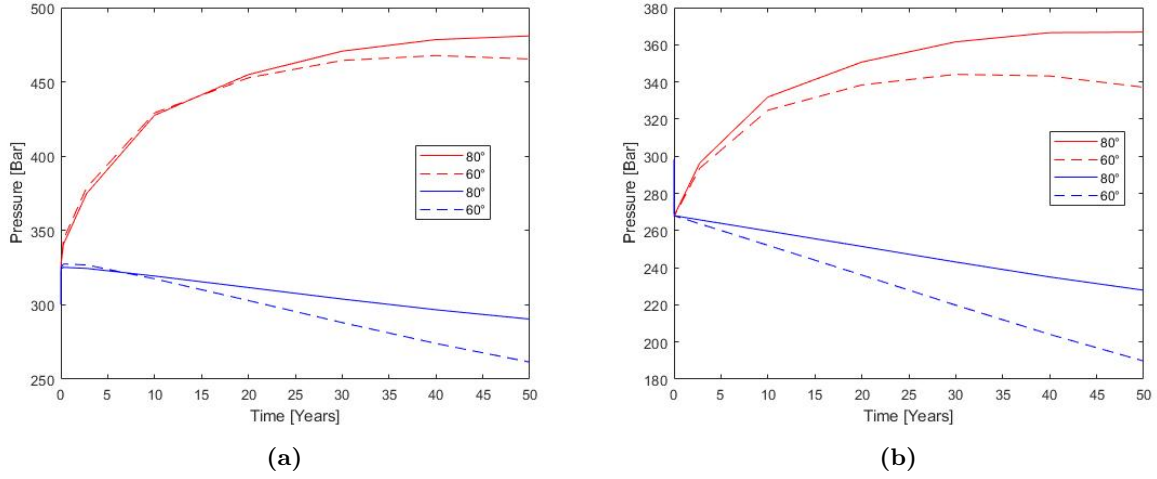
Figure 25: **(a)** The effect of the $60°$C injection temperature on the pressure at the injection point, with the CO_2 injection in red and water in blue. **(b)** The effect of the $60°$C injection temperature on the pressure at the production point, with the CO_2 injection in red and water in blue.

And the total mass of CO_2 remained unaffected by the change (figure 26).
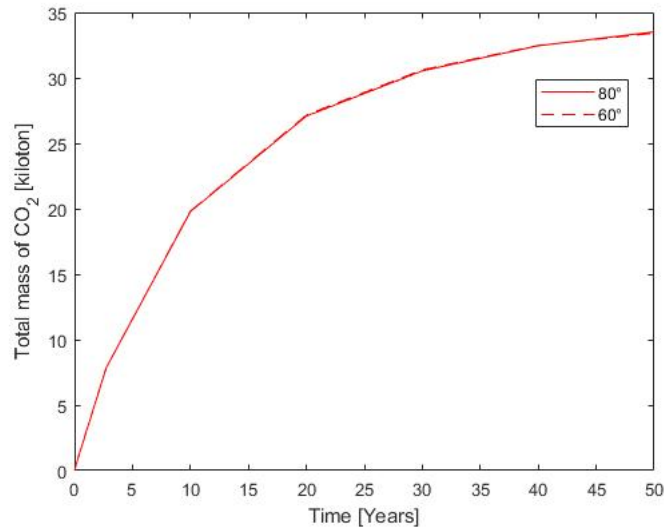
Figure 26: The effect of the $60°$C injection temperature on the total amount of CO_2 stored.

5.6 The effect of permeability

Increasing the permeability did not affect the heat production (figure 27a) but did slightly decrease the temperature at the production point (27b).
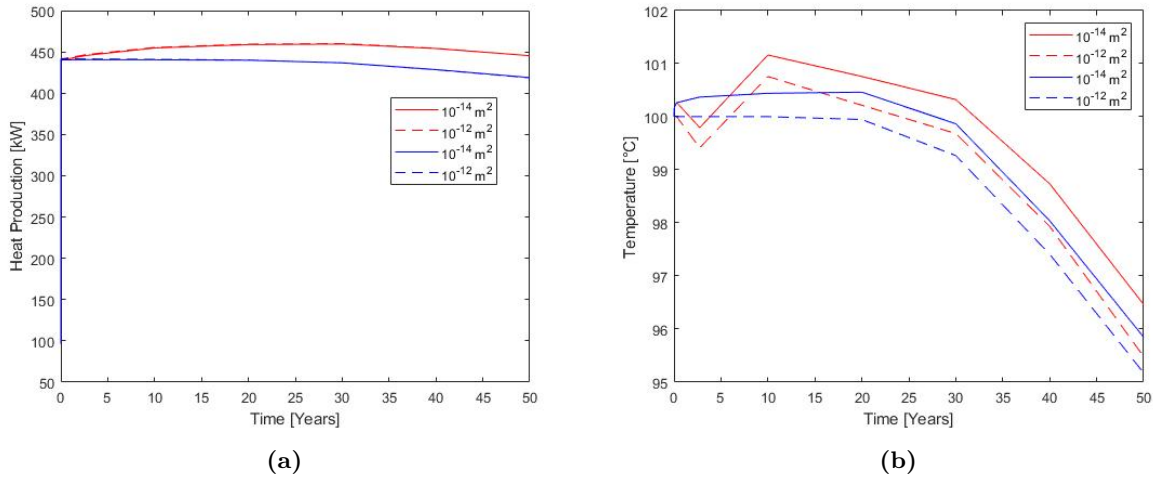
Figure 27: (a) The effect of the 10^{-12} m^2 permeability on the heat production, with the CO_2 injection in red and water in blue. **(b)** The effect of the 10^{-12} m^2 permeability on the temperature at the production point, with the CO_2 injection in red and water in blue.

The pressure at the injection point saw an decrease for both injection scenarios (figure 28a), while the production point showed the opposite behaviour (figure 28b).
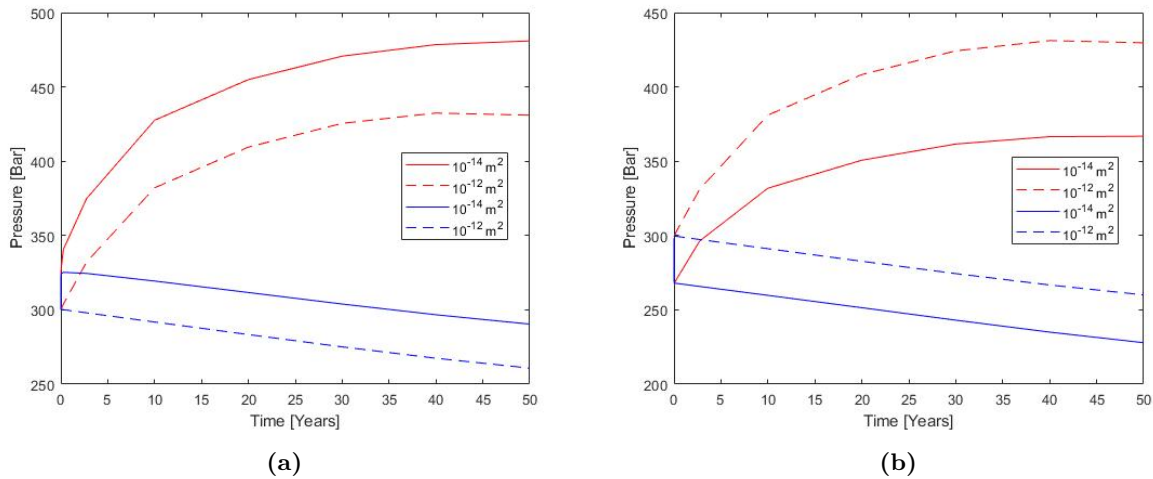
Figure 28: (a) The effect of the 10^{-12} m^2 permeability on the pressure at the injection point, with the CO_2 injection in red and water in blue. **(b)** The effect of the 10^{-12} m^2 permeability on the pressure at the production point, with the CO_2 injection in red and water in blue.

25

The total mass of CO_2 saw a slight increase as seen in figure 29.
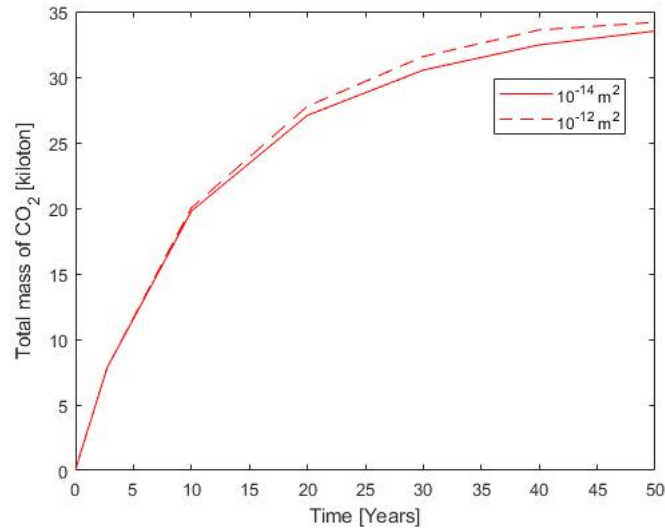
Figure 29: The effect of the 10^{-12} m^2 permeability on the total amount of CO_2 stored.

5.7 The effect of pressure

Lowering the background pressure with 100 bar represented having a more shallow rock zone, and was perhaps the least effected of all the scenarios. The heat production (figure 30a) and the temperature at the production point (30b) was both barely decreased compared to the base case scenarios.

(a)

(b)
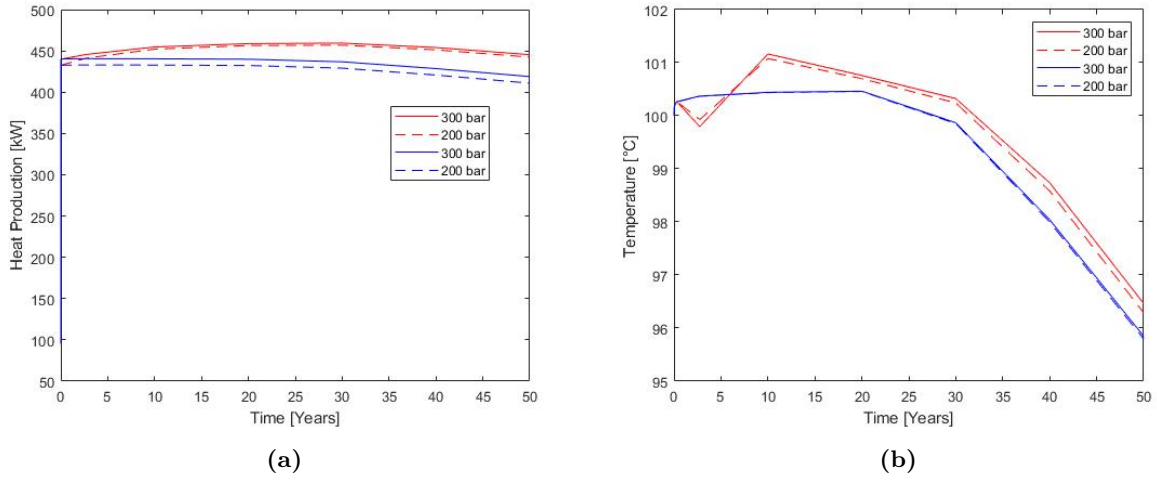
Figure 30: (a) The effect of 200 bar on the heat production, with the CO_2 injection in red and water in blue. **(b)** The effect of 200 bar on the temperature at the production point, with the CO_2 injection in red and water in blue.

The pressure at the boreholes decreased as expected, but while the water injection went down with a 100 bar the CO_2 was less effected by the pressure drop (figure 31a and 31b).

(a)

(b)
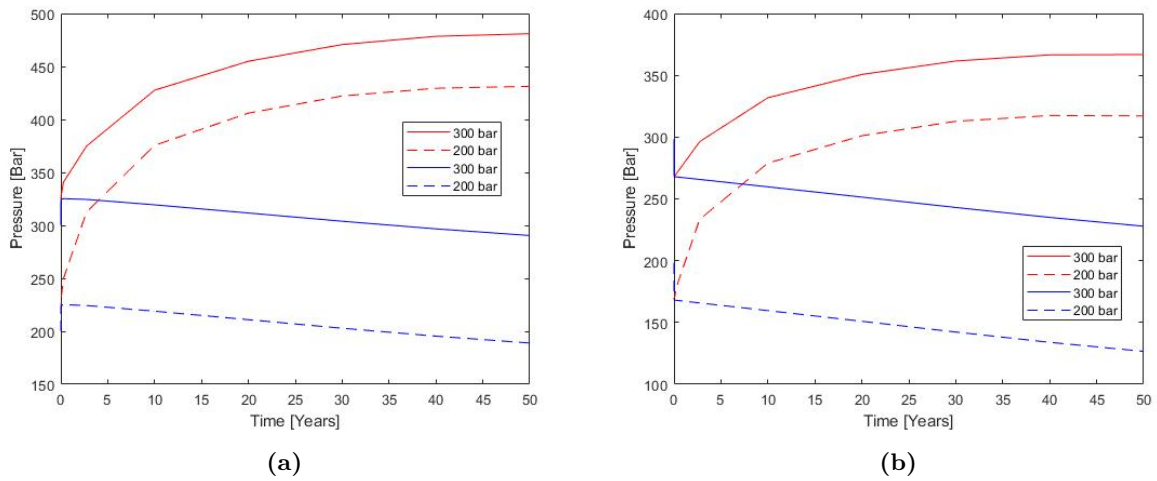
Figure 31: (a) The effect of 200 bar on the pressure at the injection point, with the CO_2 injection in red and water in blue. **(b)** The effect of 200 bar on the pressure at the production point, with the CO_2 injection in red and water in blue.

Lastly the total mass of CO_2 experienced a slight decrease as seen in figure 32.
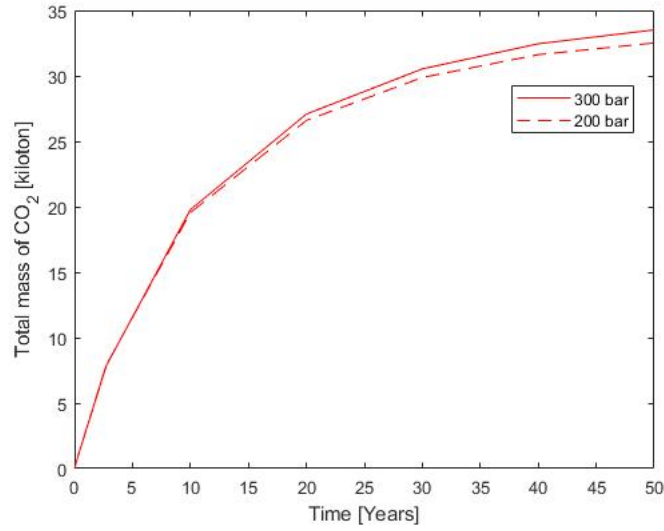
Figure 32: The effect of 200 bar on the total amount of CO_2 stored.

5.8 The effect of an initially CO_2 saturated liquid phase

The CO_2 saturated liquid phase at the simulations start only barely increased the heat production (figure 33a). The temperature at the production point on the other hand altered its initial behaviour, with the water injection looking more like the CO_2 base case scenario and the CO_2 injection scenario oscillating less (figure 33b).

(a)

(b)
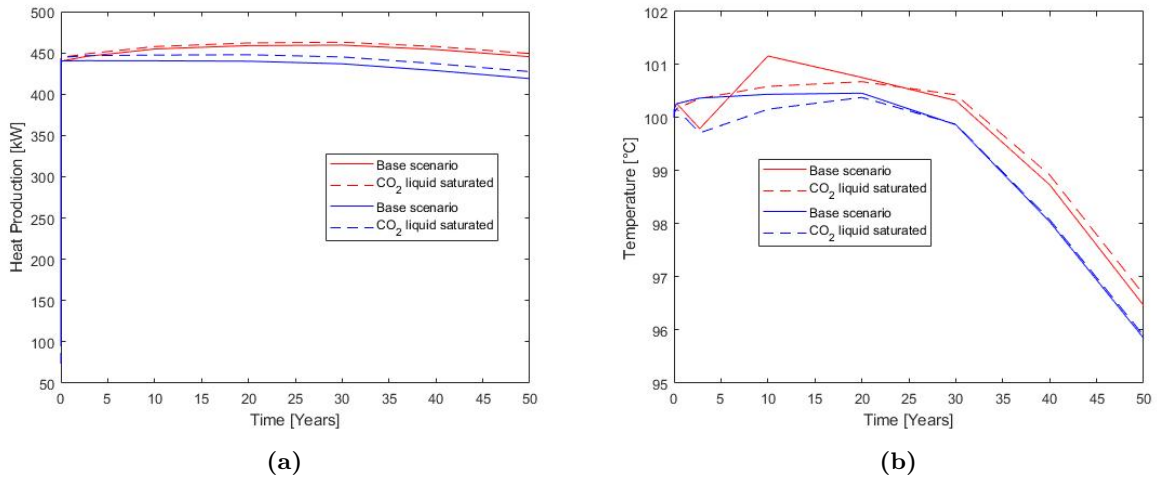
Figure 33: **(a)** The effect of an initially CO_2 saturated liquid phase on the heat production, with the CO_2 injection in red and water in blue. **(b)** The effect of an initially CO_2 saturated liquid phase on the temperature at the production point, with the CO_2 injection in red and water in blue.

Having CO_2 in the system significantly increased the overall pressure for both injection scenarios, with the most notably case being the water injection (figure 34a and 34b). This is due to the larger amount of free gas in both of the injection scenarios.
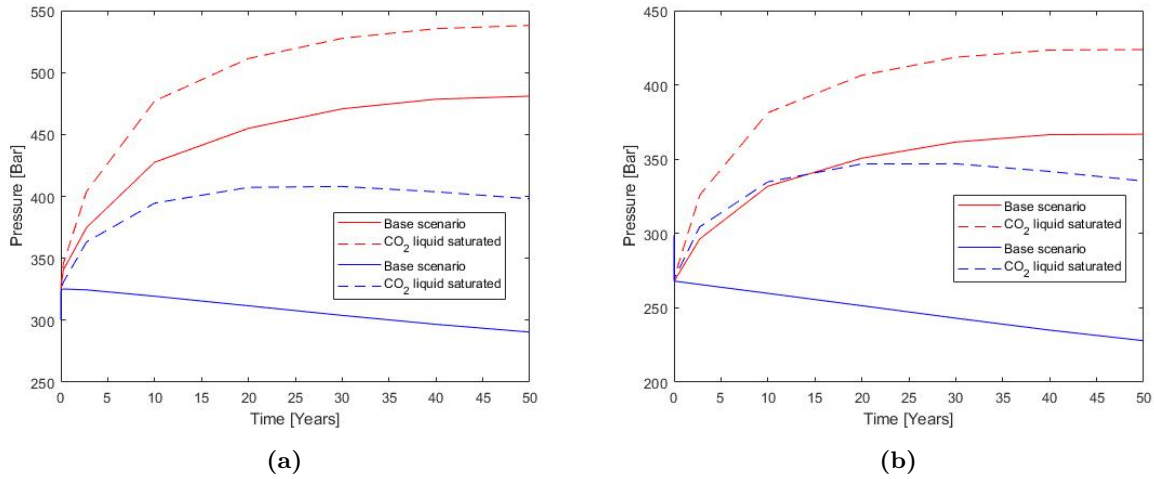
Figure 34: **(a)** The effect of an initially CO_2 saturated liquid phase on the pressure at the injection point, with the CO_2 injection in red and water in blue. **(b)** The effect of an initially CO_2 saturated liquid phase on the pressure at the production point, with the CO_2 injection in red and water in blue.

With a saturated liquid phase, the system initially has over 10 kilotons of CO_2. While allowing for a slightly higher final total mass for the CO_2 injection, the potential for storage has decreased heavily. The water injection of the other hand showed an complete washout of CO_2 after 40 years of simulation time (figure 35).
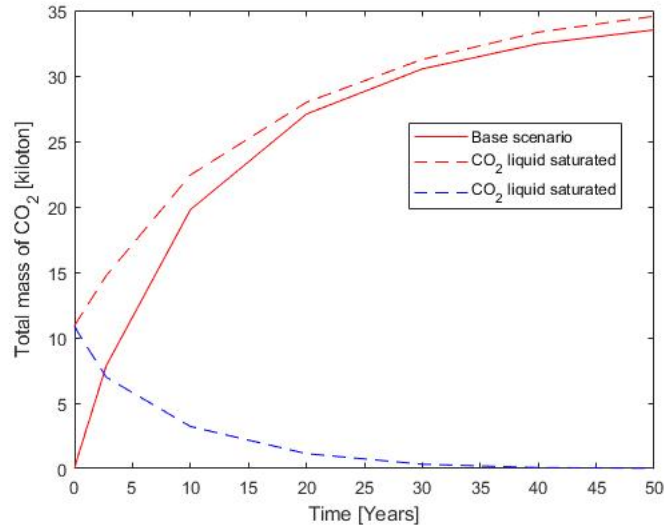
Figure 35: The effect of an initially CO_2 saturated liquid phase on the total amount of CO_2 stored, with the CO_2 injection in red and water in blue.

6   Discussion

The main focus of this study was to examine the effects of using CO_2 in the injection fluid for a geothermal system. As seen in figure 3a the heat production seems to benefit by increasing around 1-5 % throughout the simulation time.

When using the CO_2 (3a) the temperature at the production well (figure 3b) rose beyond the pure water injection after about seven years of production. This correlates to when the CO_2 is first detected at the production point, and the temperature elevation is kept throughout the simulation after this time. This is due to the two phase flows altered heat capacity, allowing for a higher heat transport. The contour plots between the two injections (figure 4 and 5) would appear almost identical. Since this temperature difference is small however, it might be of lesser concern than the pressure as discussed below.

Figure 4 and 5 also shows the flow path taken through the system. The area with lower temperature seems to have stabilized in the shape of a drop, flowing circularly outwards from the injection point and reaching its tail towards the production point. According to the Geological Survey of Sweden the expected lifespan of a geothermal plant with boreholes 1 km apart is 25 - 30 years, which is when the temperature drop from the injection point reaches the production point (SGU 2019). This approximates roughly to the behaviour seen in the contour plots.

For pressure we see the first clear drawback of using CO_2 in the injection fluid. The pressure increases over 50 % at the injection point and over 20 % at production point (figure 6a and 6b). Too high pressure increase could lead to uncontrolled fracturing resulting in unexpected flow paths and decreased performance of the geothermal system, and should be avoided. Since this pressure limit is unique to each geological system, models would have to be used for real sites to estimate the highest allowed pressure as to not over exceed it.

At the end of the simulation over 30 kilotons of CO_2 remained in the system. The total mass curve as seen in figure 10 appears to be converging at the end of the simulation, which corresponds to how the fracture zone is being filled out with free gas as seen in the gas saturation contour plot in figure 9. This amount of CO_2 might be seen as little, for instance when compared to the over 500 kilotons of CO_2 released in the iron and metal industry in Sweden each year (Naturvårdsverket 2019). However, the geological system in this study is small compared to its real life counterparts and the storage space will therefore be equally increased for such real systems. That said, the CO_2 *stored* in the system is simply what is present in any phase, mobile or trapped. This study will not quantify how much is actually trapped, so one should expect a lesser storage value then the total mass present.

Altering the injection and production rate simple increased and decreased the heat production as the rate did, although making the CO_2 and water injection indistinguishable at the lowest rate (figure 11a). The temperature at the production point generally went down faster the higher the flow rate, which is due to the colder fluid from the injection point reaching the production point at a faster rate. The 10 % CO_2 injection kept its slightly higher temperature offset compared to the water injection for the 0.6 and 1.0 kg/s flow rate scenarios.

The pressure increased as the CO_2 injection rate went up due to the faster build-up of free gas, with the pressure increasing linearly for the lowest rate and converging slowly for the two higher. This is in stark contrast to the pressure for the water injection which linearly decreased and steeper so as the injection rate went up. This is because of the lack of free gas and reverse thermal expansion, the latter due to the faster cooling of the fracture zone as the flow rate increased.

The total mass of CO_2 stored in the system sees a declining rate of return as the injection rate goes up, as seen in figure 15. This is most likely due to the restraints of the systems volume, with the higher injection rates faster filling up the available space faster and therefore converging more rapidly.

Another interesting note is the lower proportion of gas for the 0.6 kg/s CO_2 injection rate as seen in the contour plot (figure 14). The gas saturation now only reaches a maximum of 15 % and does not fill out as much of the fracture zone during each time print compared to the contour plot for the CO_2 base case scenario (figure 9).

Reducing the CO_2 injection percentage to 6 % made the heat production curve position itself between the 10 % and the pure water injection, as one might expect (figure 16a). The temperature curve at the production point showed as similar behaviour to that of the base case scenario but with a delayed and lower peak of temperature, again as one might expect with the lower injection concentration. The temperature drop at the simulations end matches the base case scenario and is likely due to the temperature drop from the injection point finally reaching the production point (figure 16b).

When looking at the contour plot for the 0.6 kg/s injection rate and the 6 % CO_2 injection concentration (figure 12 and 17) one will find them almost if not indistinguishable. This might suggest that the temperature of the system is more effected by the total amount of CO_2 injected, rather than the injection rate.

The pressure for the 6 % CO_2 injection concentration showed an altered behaviour unlike both the pure water and the 10 % CO_2 injection. The pressure starts be decreasing during the first 5 years at both the injection and production point, to then slowly climbs throughout the simulation (figure 18a and 18b). More cases with different percentages should be tested to verify the behaviour, and to possibly find the optimal injection concentration to maximize the heat production and CO_2 storage while minimizing the pressure increase.

The gas saturation in the contour plot for the 6 % CO_2 injection concentration once more reaches 20 % of the pore space while covering an area similar to that of the 0.6 kg/s (figure 19 compared to figure 14). This suggest that the injection rate determines the gas saturation while the concentration effects the spread, but should be verified with more runs with different rates and concentrations and might due to model assumption rather than reflecting reality. Finally the total mass at simulation end only reaches 53 % to that of the CO_2 base case scenario, despite having 60 % of the injection concentration (figure 20). This might be due to the higher production rate relative to the injection concentration, removing the greenhouse gas faster than it can spread compared to the base case scenario.

While only increasing heat production, temperature at production well and total mass of CO_2 slightly, introducing 3 % salinity made the pressure at both boreholes increase dramatically (figure 22a and 22b). This could be one of the examined parameters most interesting to investigate further.

Decreasing the injection temperature on the other hand barely decreased the heat production and total mass of CO_2 stored, while hastening the temperature drop at production point. The pressure was lowered at both boreholes, likely because of reversed thermal expansion due to the faster cooling. This might argue for having the lower injection temperature, keeping the benefits of the heat production and CO_2 stored while lessening the pressure strain on the system. The faster cooling will however shorten the lifespan of the geothermal system.

Increasing the permeability did not affect the heat production, and only slightly increased the total amount of CO_2. The pressure at the injection point was smaller in comparison to the base case scenario, which might be explained by the fluids enhanced ability to flow from the borehole. More strangely however was the effect on the temperature and pressure at the production point (figure 27b and 28b). While the temperature went down compared to the base case scenarios, the pressure went up instead of down as one might have expected!

Decreasing the background pressure with a 100 bar in the entire rock zone corresponds to having a more shallow depth to the zone. This scenario was the least effected, with only slightly lowered heat production, temperature at production point and total mass of CO_2 stored. The pressure at the injection and production point showed a diverging behaviour between the injection scenarios, with the water injection case dropping by 100 bar but with the CO_2 injection case only decreasing roughly 50 bar compared to the base case scenarios (figure 31a and 31b).

The final scenario investigated the effects of an initial CO_2 liquid saturated phase. While the heat production saw a slight increase, the temperature curves mirrored the opposite base case scenario for the first 5 years of simulation time to then go back to their corresponding base case scenario as seen in figure 33b. The overall pressure increased strongly for both injection scenarios (figure 34a and 34b), similar to that of having 3 % salinity scenario. As for the total amount of CO_2 stored, the pure water injection manages a complete washout of the greenhouse gas before the simulation end: Injecting CO_2 gave a slightly higher final amount compared to the base case scenario (figure 35, but since the system already had over 10 kilotons CO_2 at the simulations start the overall storage potential had gone down.

For further considerations, one might want to focus on only a few scenarios and then look carefully at many configurations of those. The injection concentration for CO_2 could be tested for 1, 2, 4, 6, 8 and 10 % for instance and the injection rate could go beyond 1 kg/s up to 10 kg/s. Salinity could be tested for more values between 0 to 10 % and having salt in the injection brine could be very interesting since this is often the case for recirculated injection fluids. The effect these parameters will have on the dissolved and gaseous CO_2 and the pressure in the system should be evaluated especially. Lastly sensitivity analysis should be performed to test the models integrity.

7 Conclusion

By comparing the pure water injection against the 10 % CO_2 injection the following could be observed:

- The heat production and temperature at the production point was increased while using CO_2. The pressure increased significantly in the fracture zone, over 50 % at the injection point and over 20 % at the production point.

- At the simulation end, about 33.5 kilotons of CO_2 remained in the system.

- Of the comparative scenarios, changing the CO_2 injection concentration and introducing salinity was the most impactful ones. By changing the concentration to 6 % the significant pressure increase observed in the 10 % CO_2 base case scenario was absent, while an almost halved CO_2 storage and a slight heat production increase remained. Introducing salinity significantly increased the pressure, while only having a small effect on the other variables.

Using CO_2 in the injection fluid does increase heat production slightly and allows for a considerable CO_2 storage, at the cost of increasing pressure in the system to a potentially dangerous degree. By varying the CO_2 injection concentration, it might be possible to avoid this large pressure increase while still maintaining the benefits and should be investigated further. Finally, further examinations regarding the injection rate and the salinity in the system and in the injection brine should be performed to better represent real life systems, and to find an optimal injection strategy to maximize heat production and CO_2 storage at an acceptable pressure increase.

References

Administration, U.S. Energy Information (2018). *Geothermal power plants*. URL: https://www.eia.gov/energyexplained/geothermal/geothermal-power-plants.php (visited on 12/02/2019).

Bonalumi, Davide, Paola A. Bombarda, and Costante M. Invernizzi (2017). "Zero Emission Geothermal Flash Power Plant". en. In: *Energy Procedia* 126, pp. 698–705. ISSN: 18766102. DOI: 10.1016/j.egypro.2017.08.302. URL: https://linkinghub.elsevier.com/retrieve/pii/S1876610217338146 (visited on 08/28/2019).

Brown, Donald William (2000). "A hot dry rock geothermal energy concept utilizing supercritical CO2 instead of water". In: Stanford University.

Cresser, Malcom et al. (2013). *Introduction to Environmental Science*. Pearson Education Limited. ISBN: 978-0-13-178932-6.

DiPippo, Ronald (2016). "Environmental Impact of Geothermal Power Plants". en. In: *Geothermal Power Plants*. Elsevier, pp. 657–684. ISBN: 978-0-08-100879-9. DOI: 10.1016/B978-0-08-100879-9.00023-9. URL: https://linkinghub.elsevier.com/retrieve/pii/B9780081008799000239 (visited on 08/27/2019).

Encyclopedia Britannica (2019). *Capillarity — physics*. en. URL: https://www.britannica.com/science/capillarity (visited on 12/27/2019).

Erlström, Mikael et al. (2016). *Geologisk information för geoenergianläggningar – en översikt*. sv. Tech. rep. Geological Survey of Sweden, p. 56.

Figueiredo, Bruno, Chin-Fu Tsang, and Auli Niemi (2020). "The influence of coupled thermo-mechanical processes on the pressure and temperature due to cold water injection into multiple fracture zones in deep rock formation".

Finsterle, S. (2007). *iTOUGH2 User's Guide*.

Francis A.L. Dullien (1988). "Two-phase flow in Porous Media". In: *Chemical Engineering & Technology* 11.1, Pages 407–424.

Fridriksson, Thráinn et al. (2016). *Greenhouse Gases from Geothermal Power Production*. Technical 009/16. ESMAP.

Goldstein, B. et al. (2011). "Great expectations for geothermal to 2100". In: *Geothermal Resources Council Annual Meeting 2011*. Vol. Volume 35 2.

IPCC (2018). *Global Warming of 1.5C*. Tech. rep. URL: https://www.ipcc.ch/sr15/ (visited on 12/28/2019).

Jelley, Nick (2017). *A Dictionary of Energy Science*. Oxford University Press. ISBN: 978-0-19-182627-6. URL: https://www.oxfordreference.com/view/10.1093/acref/9780191826276.001.0001/acref-9780191826276 (visited on 08/29/2019).

Kaya, Eylem and Sadiq J. Zarrouk (2017). "Reinjection of greenhouse gases into geothermal reservoirs". In: *International Journal of Greenhouse Gas Control* 67, pp. 111–129. ISSN: 1750-5836. DOI: 10.1016/j.ijggc.2017.10.015. URL: http://www.sciencedirect.com/science/article/pii/S1750583617305364 (visited on 08/27/2019).

Khan, Chawarwan, Robert Amin, and Gary Madden (2013). "Carbon dioxide injection for enhanced gas recovery and storage (reservoir simulation)". In: *Egyptian Journal of Petroleum* 22.2, pp. 225–240. ISSN: 1110-0621. DOI: 10.1016/j.ejpe.2013.06.002. URL: http://www.sciencedirect.com/science/article/pii/S1110062113000500 (visited on 10/04/2019).

Naturvårdsverket (2019). *Utsläpp av växthusgaser från industrin*. URL: https://www.naturvardsverket.se/Sa-mar-miljon/Statistik-A-O/Vaxthusgaser-utslapp-fran-industrin/?visuallyDisabledSeries=e20501a0888d6efc (visited on 12/13/2019).

Nick, H. M., Khaa Wolf, and David Brhun (2015). "Mixed CO2-Water Injection Into Geothermal Reservoirs: A Numerical Study". In: Melbourne, Australia: Faculty of Civil Engineering and Geosciences, Delft University of Technology.

Pruess, Karsten (1987). *TOUGH USER'S GUIDE*. Tech. rep. University of California: Lawrence Berkeley National Laboratory.

– (2005). *ECO2N: A TOUGH2 Fluid Property Module for Mixtures of Water, NaCl,and CO2*. en. Tech. rep. LBNL–57952, 877331, LBNL–57952, 877331. DOI: 10.2172/877331. URL: http://www.osti.gov/servlets/purl/877331-1FShin/ (visited on 08/21/2019).

– (2006). "Enhanced geothermal systems (EGS) using CO2 as working fluid—A novel approach for generating renewable energy with simultaneous sequestration of carbon". In: *Geothermics* 35.4, pp. 351–367. ISSN: 0375-6505. DOI: 10.1016/j.geothermics.2006.08.002. URL: http://www.sciencedirect.com/science/article/pii/S0375650506000460 (visited on 08/27/2019).

Pruess, Karsten, Curt Oldenburg, and George Moridis (2012). "TOUGH2 USER'S GUIDE, VERSION 2". en. In: p. 210.

Saldaña, Alex Grey M et al. (2016). "Numerical Simulation of Mixed Brine-CO2/H2S-Rock Interaction During the Reinjection of Non Condensable Gases". en. In: *Fortieth Workshop on Geothermal Reservoir Engineering*. Stanford University, p. 13.

SGU (2019). *Geotermi*. URL: https://www.sgu.se/samhallsplanering/energi/fornybar-geoenergi-och-geotermi/geotermi/ (visited on 12/13/2019).

Spycher, Nicolas and Karsten Pruess (2005). "CO2-H2O mixtures in the geological sequestration of CO2. II. Partitioning in chloride brines at 12–100C and up to 600 bar". en. In: *Geochimica et Cosmochimica Acta* 69.13, pp. 3309–3320. ISSN: 00167037. DOI: 10.1016/j.gca.2005.01.015. URL: https://linkinghub.elsevier.com/retrieve/pii/S0016703705000669 (visited on 02/17/2020).

Stacey, R. W., L. Norris, and S. Lisi (2016). "OLGA Modeling Results for Single Well Reinjection of Non-Condensable Gases (NCGs) and Water". en. In: p. 10.

Toth, Aniko and Elemer Bobok (2017). "Chapter 1 - What Is Geothermal Energy?" In: *Flow and Heat Transfer in Geothermal Systems*. Ed. by Aniko Toth and Elemer Bobok. Oxford: Elsevier, pp. 1–19. ISBN: 978-0-12-800277-3. DOI: 10.1016/B978-0-12-800277-3.00001-3. URL: http://www.sciencedirect.com/science/article/pii/B9780128002773000013 (visited on 09/02/2019).

Wu, Yu-Shu (2016). "Multiphase Fluids in Porous Media". en. In: *Multiphase Fluid Flow in Porous and Fractured Reservoirs*. Elsevier, pp. 15–27. ISBN: 978-0-12-803848-2. DOI: 10.1016/B978-0-12-803848-2.00002-7. URL: https://linkinghub.elsevier.com/retrieve/pii/B9780128038482000027 (visited on 09/11/2019).

Zhang, Liang et al. (2014). "Potential assessment of CO2 injection for heat mining and geological storage in geothermal reservoirs of China". In: *Applied Energy* 122, pp. 237–246. ISSN: 0306-2619. DOI: 10.1016/j.apenergy.2014.02.027. URL: http://www.sciencedirect.com/science/article/pii/S0306261914001639 (visited on 08/27/2019).